HYPERSPECTRAL REMOTE SENSING APPLICATIONS

Hyperspectral remote sensing in mineral exploration

A mineral is an element or chemical compound that is normally crystalline and that has been formed as a result of geological processes.

a naturally occurring solid chemical substance formed through bio-geochemical processes, having characteristic chemical composition, highly ordered atomic structure, and specific physical properties.

The main factors that influence the reflectance characteristics of a substance are:

- **Chemical composition**
- **Texture / particle size**

In geology, we refer to rocks as aggregates of minerals. Hence, reflectance depends on mineral composition and degree of weathering

Wavelength Range	Observable
	Minerals
0.4-1.4	Fe Bearing Minerals, Carbonates, Sulphates
1.5-1.85 2.0-2.5	Carbonates and OH groups of carbonates, Phyloosilicates, clay etc
	Vegetation
0.43-0.65 0.90-1.40 1.40-1.90 2.00-2.40	Chlorophyll a+b pigments Plant water content, cellulose Protein, starch, lignin Starch, protein, nitrogen, cellulose
	Snow and Ice
0.4-0.8 0.8-1.4	Snow grain size, snow depth, contaminents Snow grain size, liquid water content

Requirement of Spectral resolution is determined by the width of the occurring absorptions. For Soils and Geological investigations mostly in the near and short wave infrared a 10mm resolution is necessary

Bands	Band width	Application
445nm-670nm	10-20 nm	Vegetation/Water/ Fe-Minerals
683nm – 720 nm	5-10 nm	Vegetation
745nm-765nm	5-10nm	Vegetation/Atmos pheric correction
780nm	5-10nm	Vegetation/Fe-minerals
880nm-1035nm	5-10nm	Vegetation/Fe-minerals

Soils and Rocks

	SWIR 1500-1800nm	Optimum Spectral resolution
Determination of Soil Moisture		<= 50nm
Weak absorption bands of carbonates Dolomite and calcite	1740nm 1760nm	10nm 10nm
	SWIR 2000-2400nm	
Characteristics absorption bands of Carbonate, -OH and sulphate bearing minerals Broad CO3 bands in carbonates, calcite, Dolomite OH and AlOH bearing minerals – Kalonite, Muscovie, Aluniteat etc	At 2320 nm At 2310nm 2200nm 2300nm	10nm 10nm 10nm 10nm

Role of Remote sensing in mineral exploration

- Mapping regional lineaments and structural trends
- Mapping local fracture patterns
- Detecting hydrothermally altered rocks
- Providing basic geologic data

GEOLOGICAL GUIDES FOR PROSPECTING

There are several geological guides for prospecting that can be observed on remotely sensed data. These include the following:

1) Stratigraphical-Lithological
2) Geomorphological
3) Structural
4) Rock Alteration
5) Geobotanical

Hyperspectral > Another Empirical Data Layer for Prospectivity Analysis

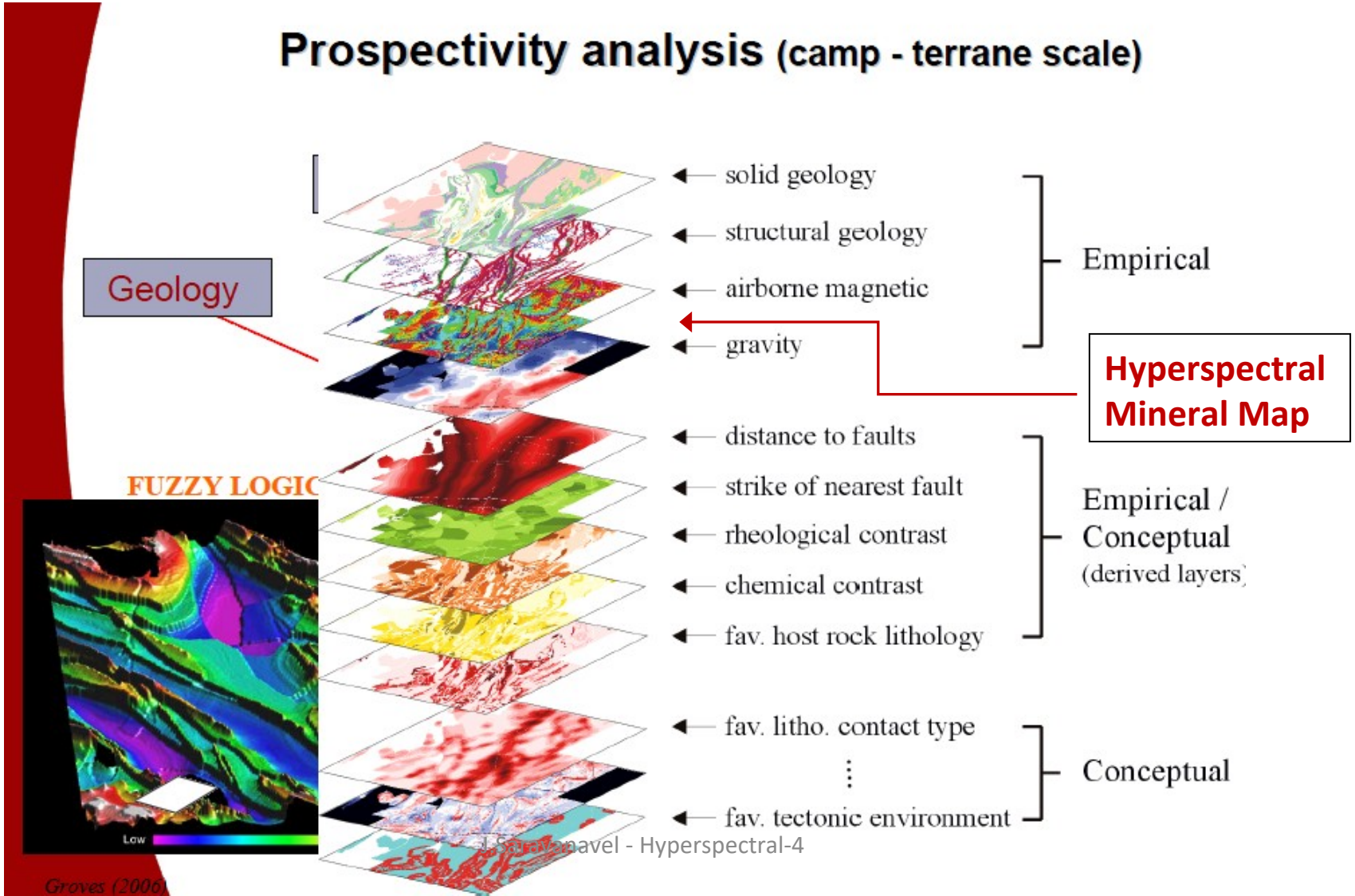

Hydrothermal Wall rock alteration

The wall-rock alteration is quite common in case of hydrothermal deposits.

The nature of mineralizing solution like its chemical character, temperature and pressure as well as character and kind of wall rock decide about the nature and intensity of alteration. Sericitization, kaolinisation and silicification are the common forms of alteration in the wall rock.

High temperature minerals like tourmaline, topaz and amphibole may develop. Basic and ultrabasic igneous rocks are serpentinized accompanied by the production of epidote and chlorite.

Types of Hydrothermal Wall rock alteration

Advanced argillic - characterized by the clays dickite, kaolinite and pyrophyllite (all hydrated aluminum silicates) and quartz. Sericite may be present as well as alunite and tourmaline. Alteration involves the extreme leaching of cations, especially the difficult to leach alkalis and calcium, and the concentration of H+. This type of alteration is characteristic of many epithermal precious metal deposits and a smaller number of mesothermal deposits such as Butte, Montana.

Potassic alteration - characterized by secondary *kspar + biotite*. Anhydrite may be present, but its susceptibility to solution generally results in its dissolution in near surface environments. Because it is characterized by common silicates, potassic alteration is often difficult to detect. Pyrite and minor chalcopyrite and molybdenite are the only ore minerals associated with this alteration.

Sericitization (Phyllic) - characterized by the assemblage *quartz + sericite + pyrite*. Generally the most common form of alteration. Sulfides present, in addition to pyrite, include chalcopyrite, bornite and a variety of less common copper sulfides. Generally the result of oxidation of Fe.

Argillic - characterized by *kaolinite + montmorillonite*. Somewhat similar to advanced argillic alteration, but with a lesser degree of leaching of cations. Also unlike advanced argillic alteration which is associated with vein type deposits, argillic alteration is more closely associated with disseminated deposits, porphyry coppers in particular. Sulfides are less common in association with this alteration type.

Propylitic - characterized by the assemblage *chlorite + epidote + calcite*. Albite as well as other carbonates may be present. Due to presence of the green minerals chlorite and epidote this zone is usually easily recognizable by its color. Associated sulfides include pyrite, copper sulfides, galena, sphalerite and a host of complex arsenides. Often this zone can be quite large and is useful during mineral exploration. Unlike the previous types above which are characterized by leaching of cations this zone seems to represent the addition of cations.

Silicification - characterized by quartz or chert. Can be added by solutions as is the case in many low temperature deposits or the result of complete leaching of all cations plus aluminum.

Dolomitization - addition of magnesium to limestone to form dolomite. Common in Mississippi Valley type deposits.

Other alteration types:

Feldspathization - *kspar + albite*, forms in the deep zones of some porphyry copper deposits.

Greisenization - *tourmaline + topaz + cassiterite + various tungsten-bearing minerals*. Common form of alteration on association with porphyry tin deposits.

Fenitization - characterized by *nepheline, alkali feldspar and Na-bearing amphiboles*. Hematization - characterized by secondary *hematite*.

Bleaching - not characterized by any specific mineral assemblage, but rather a color change between altered and unaltered rock. Generally the result of oxidation of Fe.

Two examples of spectral characteristics of common mineral groups is as follows.

1) Tectosilicates (quartz + feldspars).

- No absorption features in solar reflection region.
- Increased reflectance in the VNIR + SWIR region.
- Absorption features in the TIR region.
- Multispectral data in TIR region can distinguish between types of silicates.

2) Limonite (iron oxide)

leads to strong absorption in the blue-end region of the VIS spectrum.

Compound or double ratios of MSS developed to map limonite-bearing zones.

GEOLOGICALLY SIGNIFICANT REGIONS OF THE ELECTROMAGNETIC SPECTRUM

Wavelength region and range	Mineralogy	Associated molecular feature
VNIR 400-1100	Fe and Mn oxides, rare earths	Crystal field absorption, charge transfer absorption
SWIR 1100-2500	Hydroxyls, carbonates, sulphates, micas, amphiboles	$Al(OH)_2$, $Fe(OH)_2$, $Mg(OH)_2$, NH_4, SO_4 absorption, CO_3
TIR 8000-14000	Carbonates, silicates	Si-O bond distortion

ENVIRONMENT OF FORMATION	STANDARD TERMINOLOGY	SWIR ACTIVE MINERAL ASSEMBLAGE
Intrusion-related	Potassic (biotite-rich), K silicate, biotitic	Biotite (phlogopite), actinolite, sericite, chlorite, epidote, muscovite, anhydrite
	Sodic, sodic-calcic	Actinolite, clinopyroxene (diopside), chlorite, epidote, scapolite
	Phylitic, sericitic	Sericite (muscovite-illite), chlorite, anhydrite
	Intermdiate argillic, sericite-chlorite-clay (SCC), argillic	Sericite (illite-smectite), chlorite, kaolinite (dickite), montmorllite, calcite, epidote
	Advanced argillic	Pyrophillite, sericite, diaspora, alunite, topaz, tourmaline, dumortierite, zunyite
	Greisen	Topaz, muscovite, tourmaline
	Skran	Clinopyroxene, wollastonite, actinolite – termolite, vesuvinaite, epidote, serpentinite –talc, calcite, chlorite, illite –smecite, nontronite
	Propylitic	Chlorite, epidote, calcite, actinolite, sericite, clay
High – sulfidation epithermal	Advanced argilllic- acid sulphate	Kaolinite, dickite, alunite, diaspore, prophyllite, zunyite
	Argillic intermidiate argillic	Kaolinite, dickite, montmorllllite, illite-smecite
	Propylitic	Calcite, chlorite, epidote, sericite, clay

ENVIRONMENT OF FORMATION	STANDARD TERMINOLOGY	SWIR ACTIVE MINERAL ASSEMBLAGE
Low sulfidation epithemal	Adularia –sericite, sericitic argillic	Sericite, illite-smectite, kaolinite, chalcedony, opal, montmorllite, calcite, dolomite
	Advanced argillic – Acid – sulphate (steam- headed)	Kaolinite, alunite, crisobalite (opal, chalcedony), jarosite Calcite, epidote, wairakite, chlorite, illite-smectite,
	Porphylitic, zeolitic	montmorillite
Mesothermal	Carbonate	Calcite, ankerite, dolomite, muscovite (Cr- N rich)
	Chloritic	Chlorite, muscovite, actinolite
	Biotite	Biotite, chlorite
Sediment –hosted gold	Argillic	Kaolinite, dickite, illite
Volcaogenic massive sulfide	Sericitic	Seritic, chlorite, chloridoid
	Chloritic	Chlorite, sericite, biotite
	Carbonate	Dolomite, siderite, ankerite, calcite, sericite, chlorite
Sediment hosted massive sulfide	Tourmalinite	Tourmaline, muscovite
	Carbonate	Ankerite, siderite, calcite, muscovite
	Sericitic	Sericite, chlorite
	Albitic	Chlorite, muscovite, biotite

Mineral Identification	Alteration Interpretation	Exploration Application
Alunite	Advanced argillic	High – Sulfidation environment, and zoning around high sulfidation Steam-heated zones in low sulfidation
Dickite	Advanced argillic	Zoning around high sulfidation Sediment-hosted Au, with mineralization
Kaolinite	Advanced argillic and weathered rock	High-sulfidation Sediment-hosted Au, zoning
Dickite, pyrophllite, diaspore	Advanced argillic	Depth estimation
Chlorite	Propylitic, chloritic	VMS zoning Uranium zoning
Illite/smectite	Argillic	High and low sulfidation, zoning Uranium, zoning
Carbonate	Carbonate	Mesothermal, zoning

Alteration Minerals Identifiable by Hyperspectral data

- Clays: Kaolinite, Dickite, Halloysite, Pyrophyllite, Illite-Smectite, Montmorillionite
- Micas: White mica (Sericite), Illite, Phengite, Muscovite, Paragonite, Biotite, Phlogopite, Pyrophyllite, etc.
- Chlorites: Variations in Fe, Mg content
- Other Phyllosilicates: Serpentines (Lizardite, Antigorite), Fuchsite, Talc, Nontronite
- Amphiboles: Tremolite, Hornblende, Actinolite, Anthophyllite
- Carbonates: Cal+cite, Dolomite, Ankerite, Siderite
- Sulphates: Alunite, Jarosite, Gypsum
- Tourmaline: Fe-tourmaline, Tourmaline

Major Absorptions:

- Al-OH: clays, micas
- Fe-OH: chlorites, serpentines
- Mg-OH: serpentines, chlorites, micas, epidote, some amphiboles

Possible Mineral Deposits by Hyperspectral Alteration Mapping

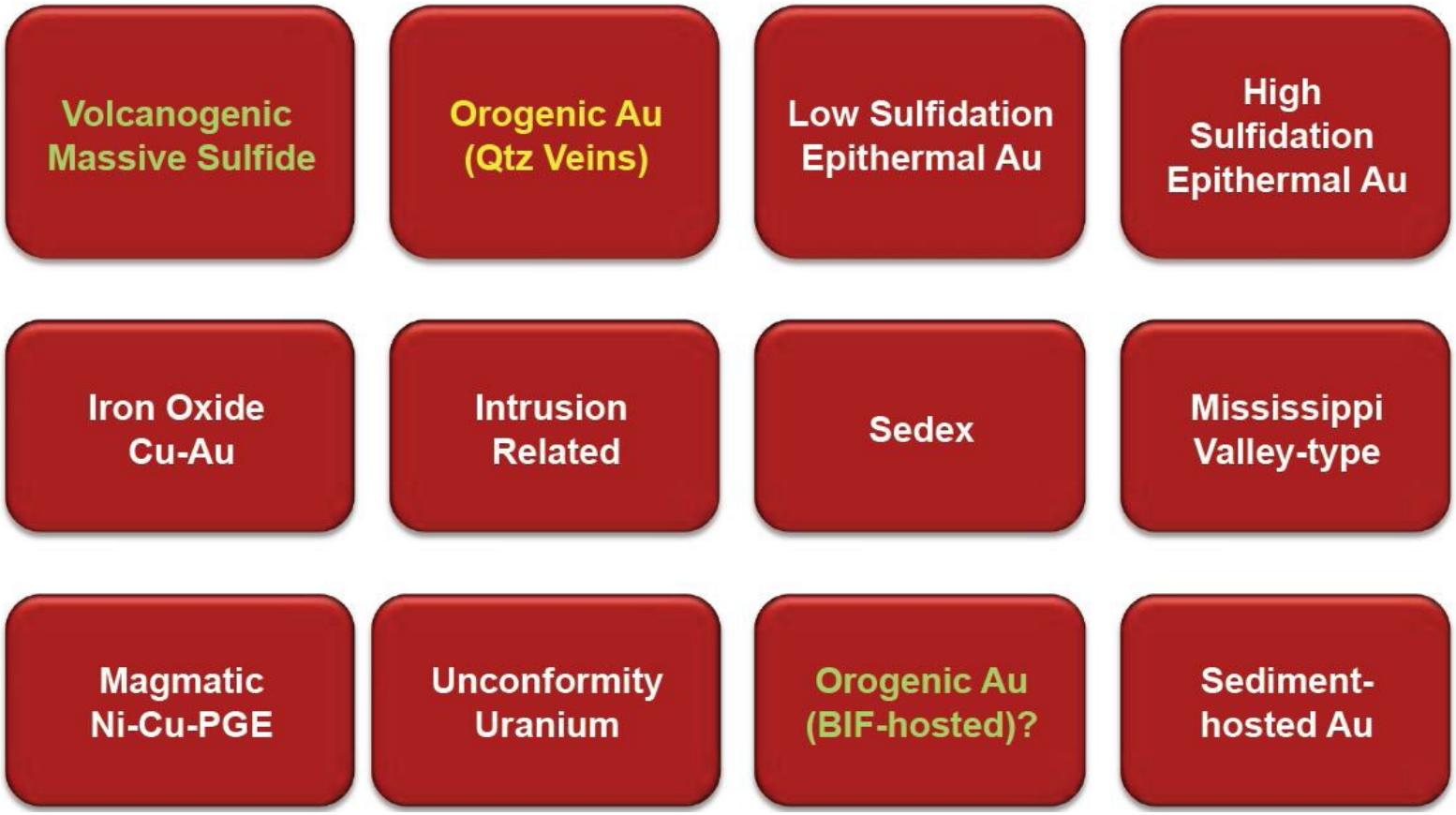

Porphyry Deposit Model – Hydrothermal Alteration Zones > Mineral Mapping

Figure: Illustrated deposit model of a porphyry copper deposit (modified from Lowell and Guilbert, 1970). A.Mineral Alteration Zones B.Mineralization/Ore Shells

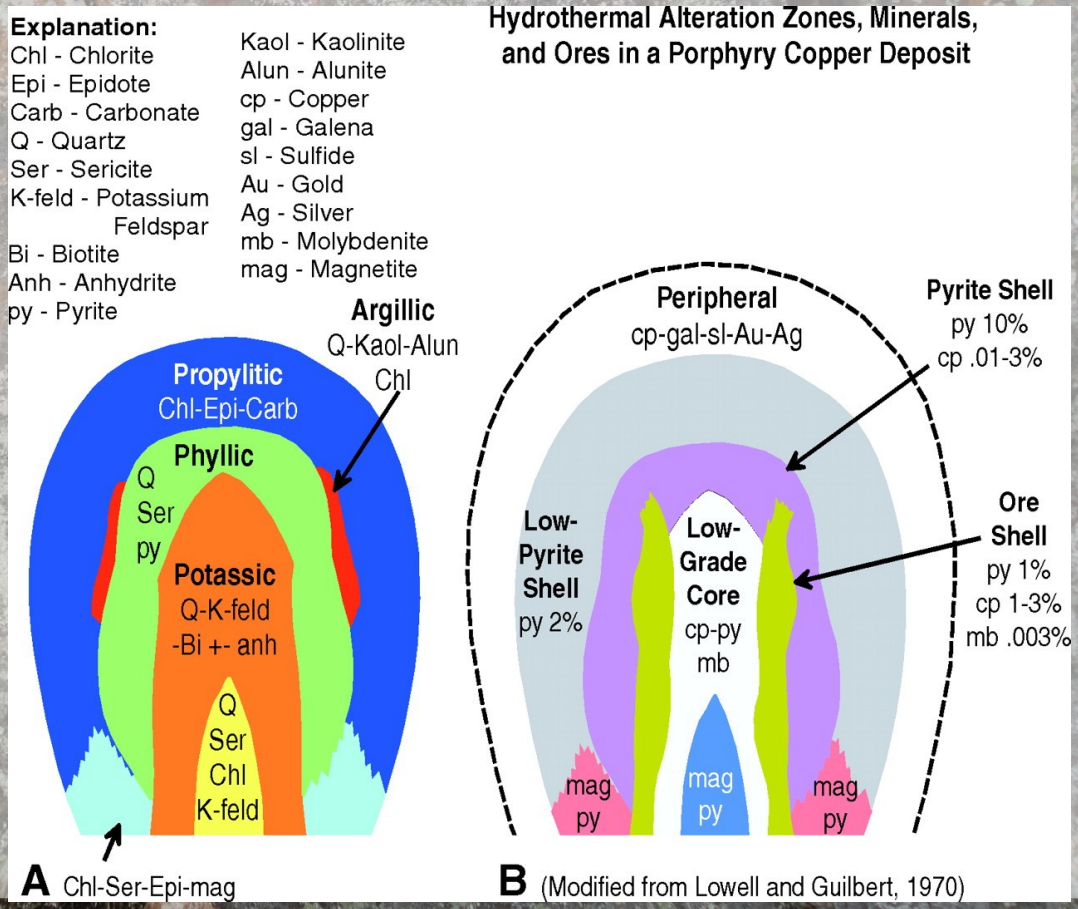

Epithermal Deposit Model – Hydrothermal Alteration Zones

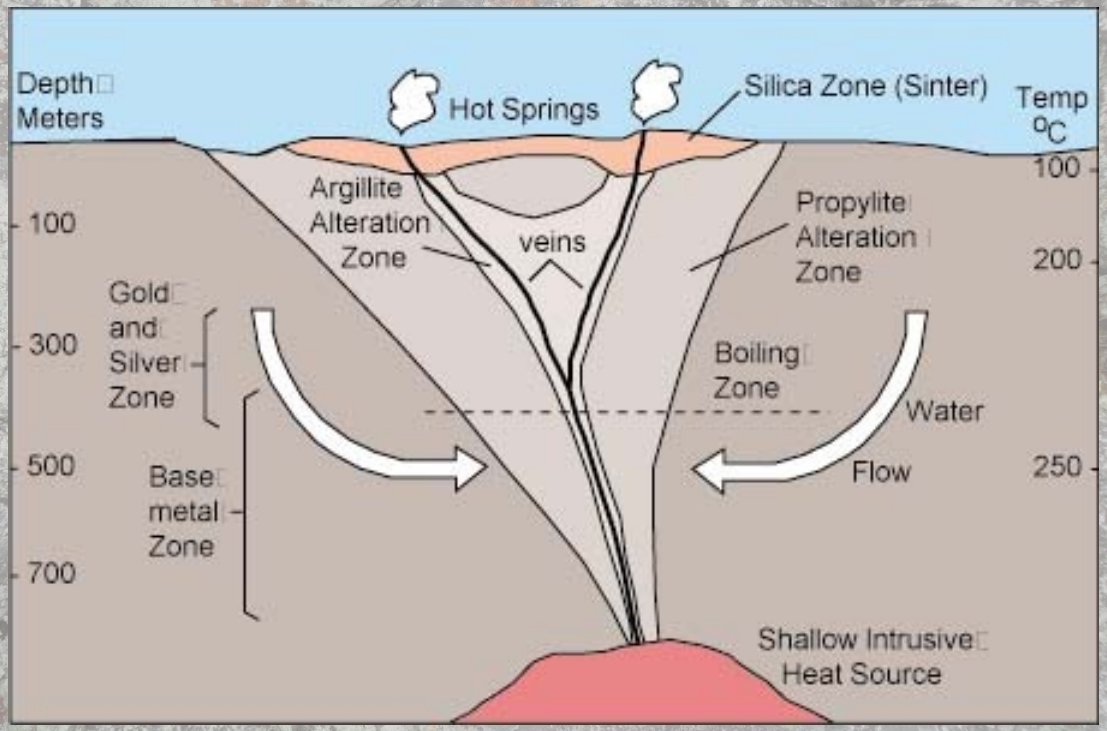

Diagram from ITAM Gold by the Minerals Council of Australia

VMS Deposits – Hydrothermal Alteration

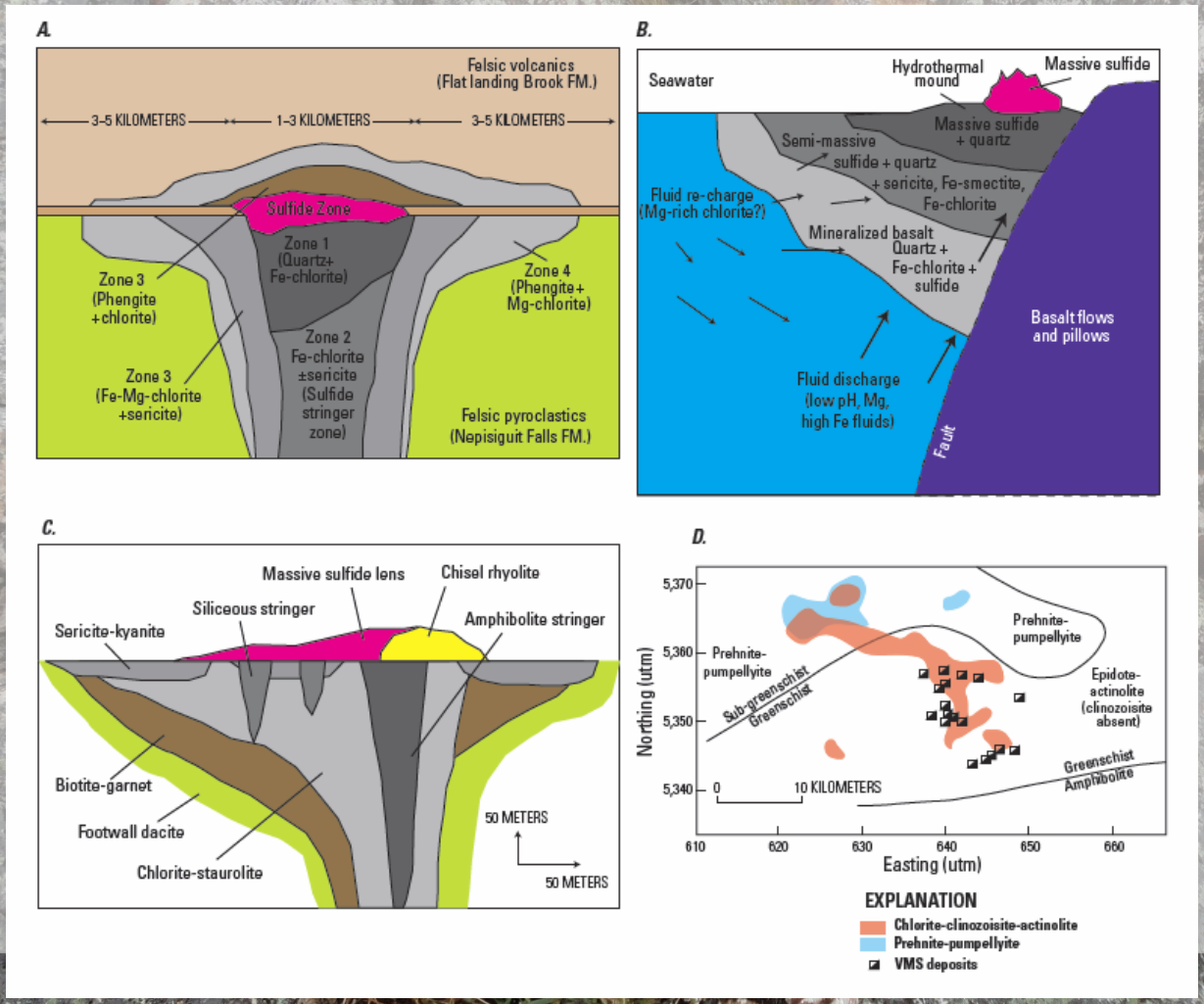

Figure: Representative examples of alteration zoning in ancient volcanogenic massive sulfide deposits.
A, Hydrothermal alteration in the Bathurst district after Goodfellow (2007).
B, Alteration in the mafic, ophiolitic Turner-Albright, OR, deposit (Zierenberg and others, 1988) shows an alteration pattern related to replacement mineralization in a porous and permeable hyaloclastite pile with general similarities to alteration at TAG and the Galapagos Rift.
C, Chisel Lake deposit in the Snow Lake district, Manitoba, where alteration has undergone amphibolite-grade regional metamorphism (Galley and others, 1993).
D, Semi-conformable alteration zones (Hannington and others, 2003) that are clearly discordant to regional metamorphic isograds in the Blake River Group, Noranda volcanic complex, western Abitibi subprovince, Ontario. [Fe, iron; Mg, magnesium; Fm., formation]

From Shanks et al., 2010 (USGS Publication: Volcanogenic Massive Sulfide Occurrence Model)

VMS Deposits – Hydrothermal Alteration

- Studies of alteration assemblages in these continental hydrothermal settings led to a series of commonly recognized alteration zones: **potassic, argillic, phyllic, and propylitic**, with distinct mineralogy and, respectively. **Decreasing intensity of alteration developed away from the vein or pluton**
- Bonnet and Corriveau (2007) retained some of these classification terms (Table 11–1) and used some of the assemblage names for VMS deposits, but **substituted sericitic for phyllic** and, like other researchers, added **chloritic as an important alteration zone in subseafloor settings**. **Advanced argillic is a special type of alteration that forms in highly acidic, high sulfidation-state conditions** characteristic of near-seafloor (or near-surface) oxidation of SO_2or H_2S to produce sulfuric acid.

Table 11–1. Diagnostic minerals in hydrothermally altered volcanogenic massive sulfide deposits at different metamorphic grades.

[Modified from Bonnet and Corriveau, 2007. Fe, iron; K, potassium; Mg, magnesium]

Alteration type	Diagnostic minerals: unmetamorphosed deposits	Diagnostic minerals: greenschist facies	Diagnostic minerals: granulite facies
Advanced argillic	Kaolinite, alunite, opal, smectite	Kaolinite, pyrophyllite, andalusite, corundum, topaz	Sillimanite, kyanite, quartz
Argillic	Sericite, illite, smectite, pyrophyllite, opal	Sericite, illite, pyrophyllite	Sillimanite, kyanite, quartz, biotite, cordierite, garnet
Sericitic	Sericite, illite, opal	Sericite, illite, quartz	Biotite, K-feldspar, sillimanite, kyanite, quartz, cordierite, garnet
Chloritic	Chlorite, opal, quartz, sericite	Chlorite, quartz, sericite	Cordierite, orthopyroxene, orthoamphibole, phlogopite, sillimanite, kyanite
Carbonate propylitic	Carbonate (Fe, Mg), epidote, chlorite, sericite, feldspar	Carbonate (Fe, Mg), epidote, chlorite, sericite, feldspar	Carbonate, garnet, epidote, hornblende, diopside, orthopyroxene

From Shanks et al., 2010 (USGS Publication: Volcanogenic Massive Sulfide Occurrence Model)

Kimberlite Pipe – Diamond Exploration

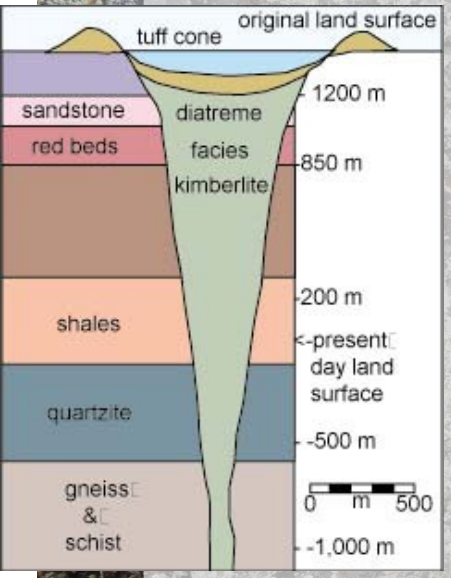

HyVista, 2011

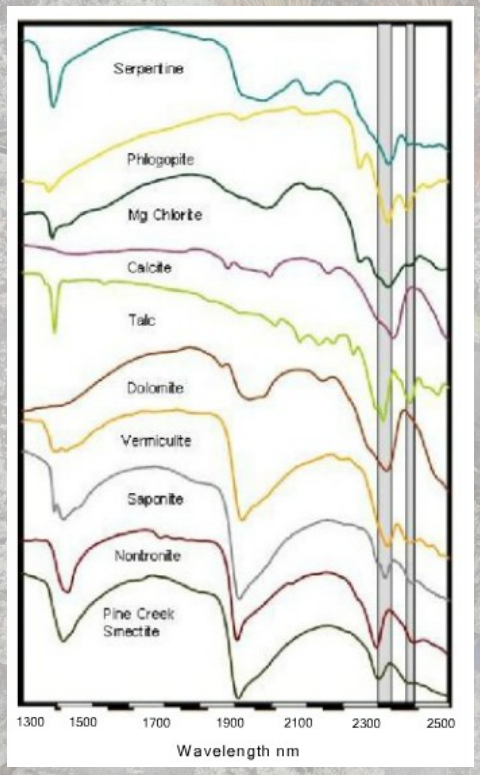

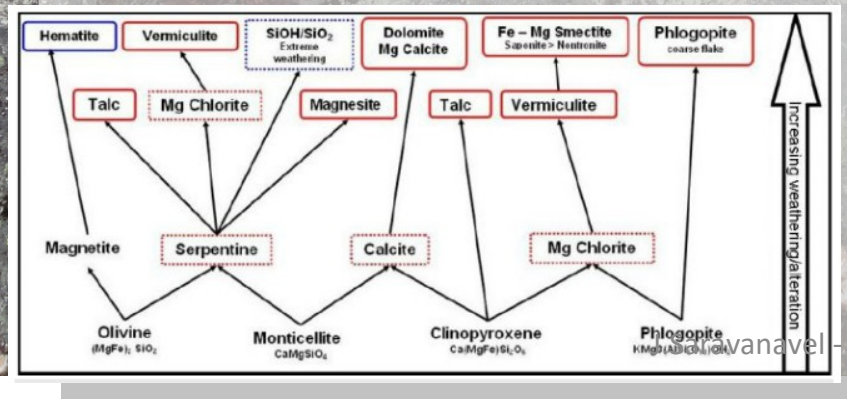

Simplified version of a Kimberlite pipe from Hawthorne (1975)

- Diamonds are brought to the surface from the mantle in a rare type of magma called kimberlite and erupted at a rare type of volcanic vent called a diatreme or pipe.
- Kimberlite is a gas-rich, potassic ultramafic igneous rock that contains the minerals olivine, phlogopite, diopside, serpentine, calcite, and minor amounts of apatite, magnetite, chromite, garnet, diamond, and other upper mantle minerals.
- Some of these minerals can be differentiated using hyperspectral imagery
  - VNIR-SWIR: olivine, phlogopite, serpentine, calcite
  - TIR: calcite, diopside, garnet, apatite, other silicates
- Challenge: pipes are small in size/diameter; mafic rocks with lower spectral signal alteration minerals

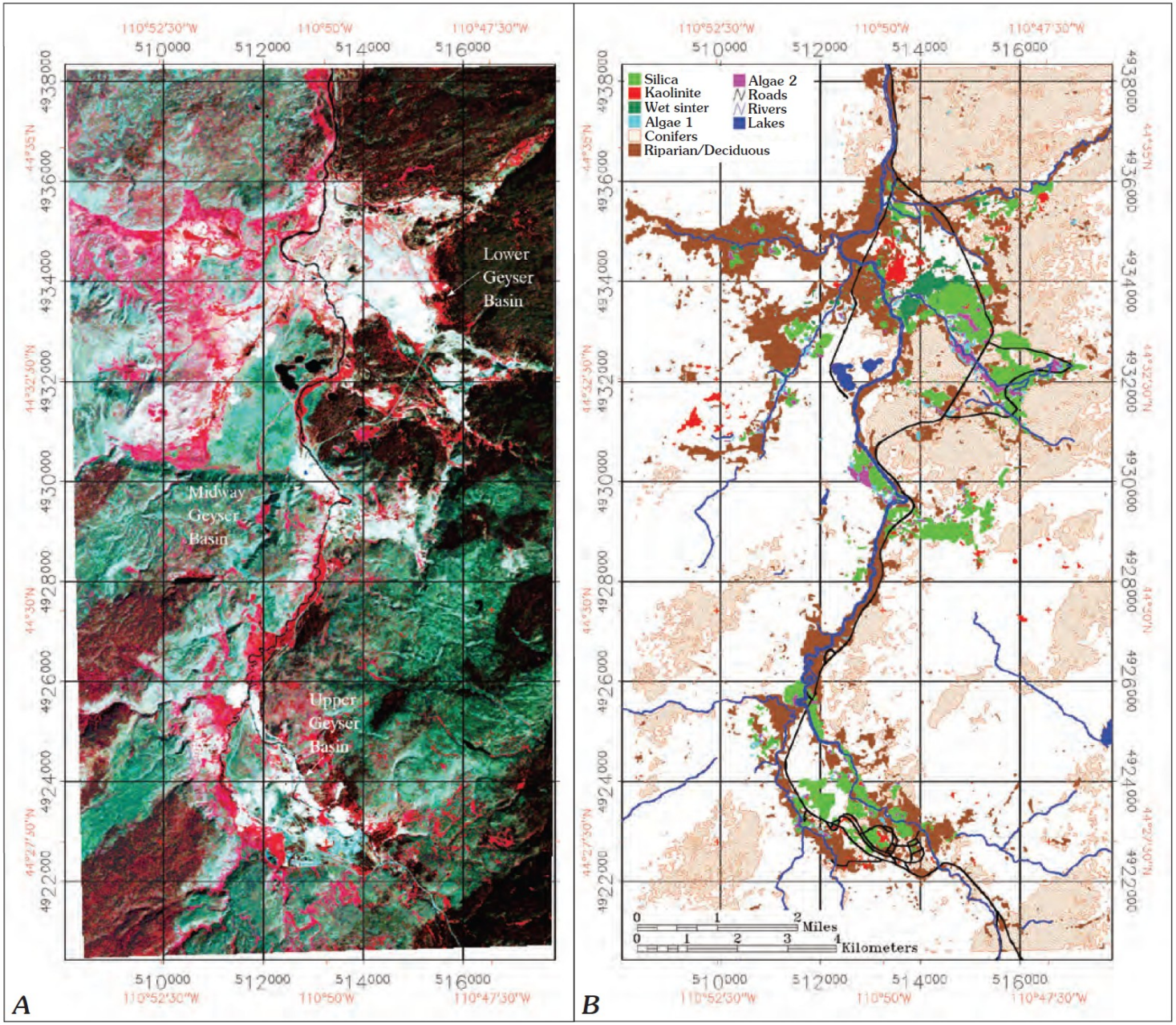

Figure 4. 1996 AVIRIS maps. *A,* false-color composite map. *B,* Derived map.

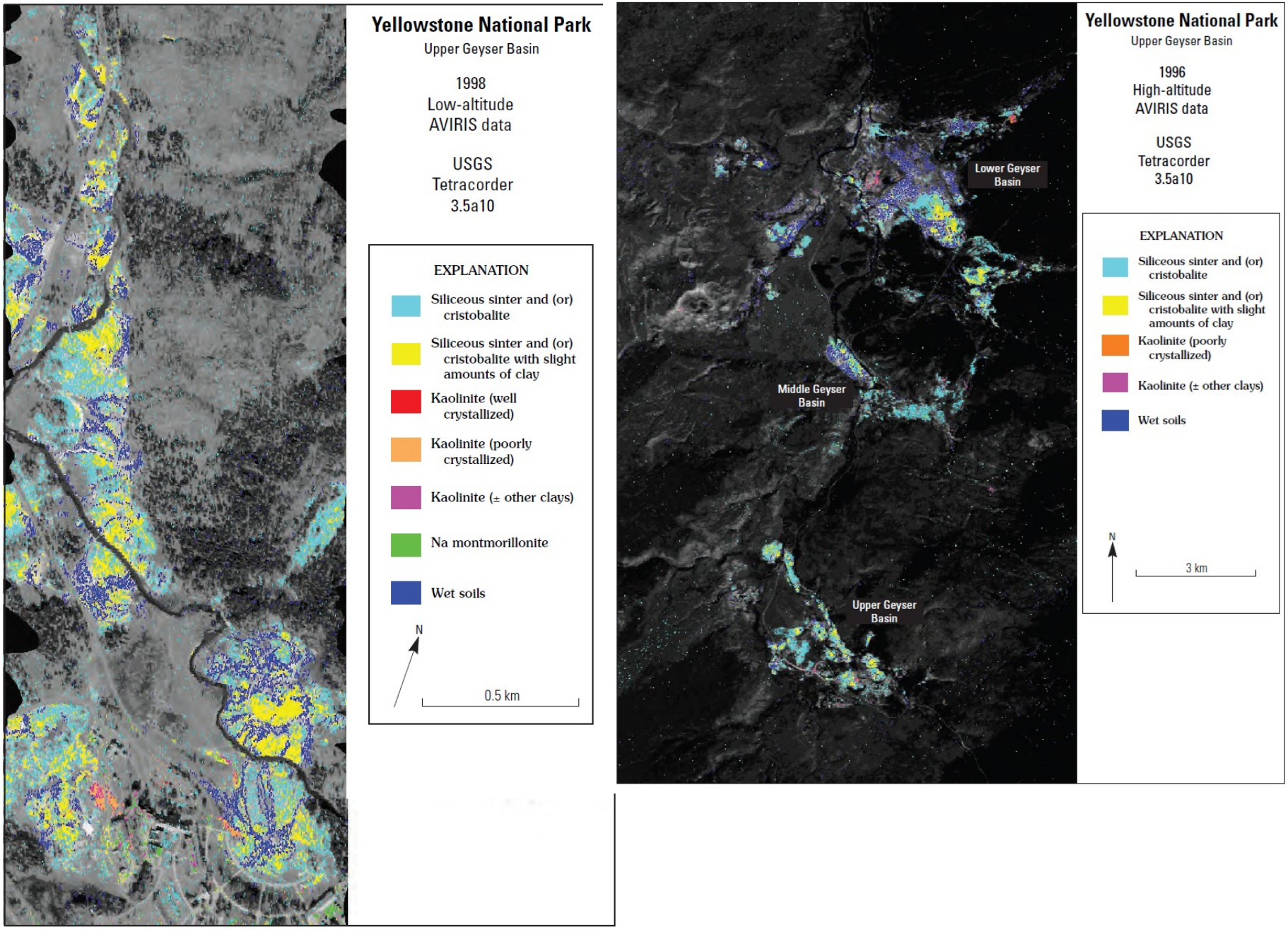

Figure 5. Mineral map of Upper Geyser Basin.

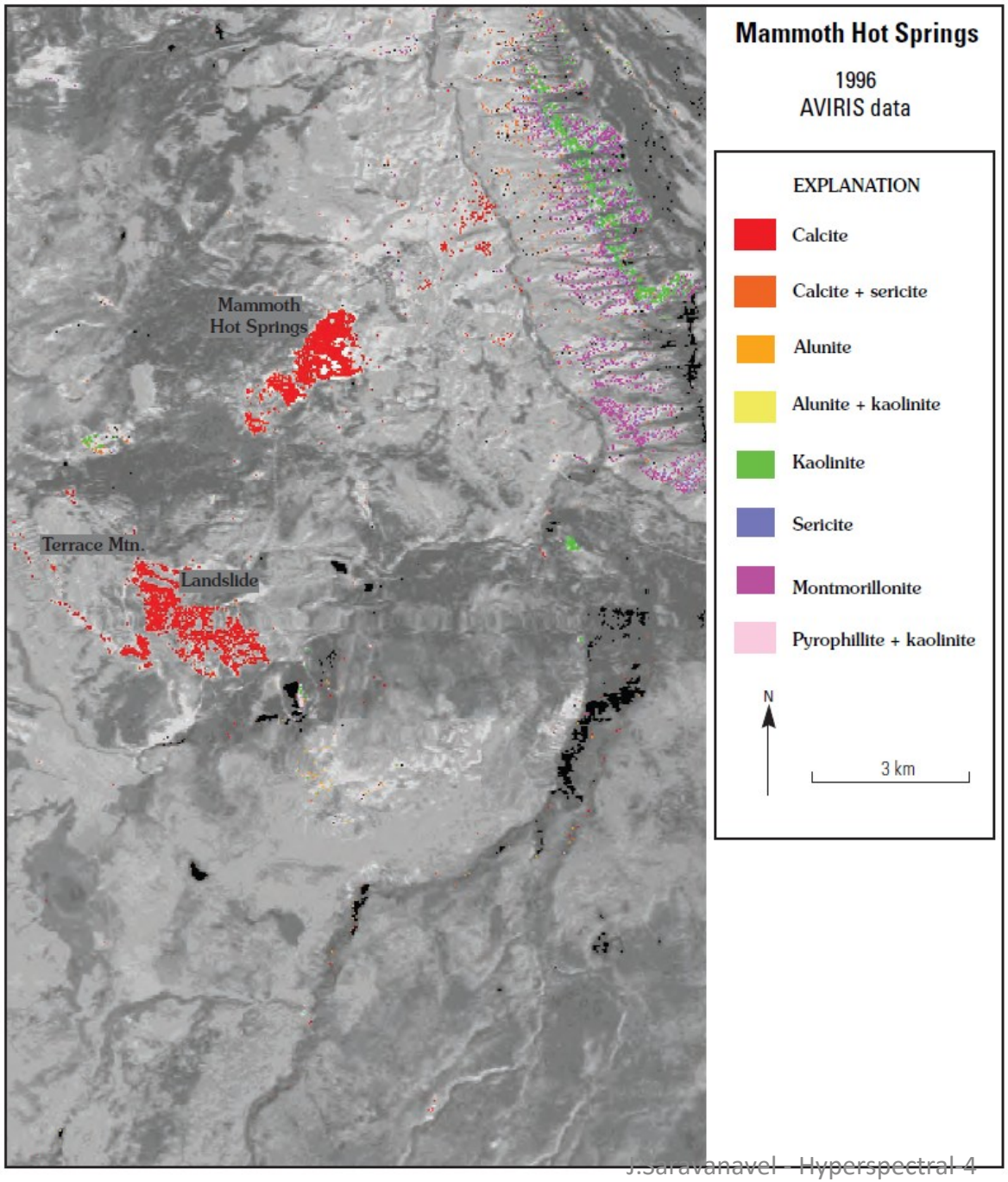

Mammoth Hot Springs is a large travertine deposit that was precipitated from water that percolated through underlying limestone bedrock. Mammoth Hot Springs and Terrace Mountain, an inactive travertine deposit to the southwest, have strong carbonate spectral features that map as calcite.

Hyperspectral Remote Sensing of Vegetation

Hyperspectral Remote Sensing of Vegetation

More specifically hyperspectral Remote Sensing, originally used for detecting and mapping minerals, is increasingly needed for to characterize, model, classify, and map agricultural crops and natural vegetation, specifically in study of

(a)Species composition (e.g., *chromolenea odorata vs. imperata cylindrica*);
(b)Vegetation or crop type (e.g., soybeans vs. corn);
(c)Biophysical properties (e.g., LAI, biomass, yield, density);
(d)Biochemical properties (e.g, Anthrocyanins, Carotenoids, Chlorophyll);
(e)Disease and stress (e.g., insect infestation, drought),
(f)Nutrients (e.g., Nitrogen),
(g)Moisture (e.g., leaf moisture),
(h)Light use efficiency,
(i)Net primary productivity

Spectral Wavelengths and their Importance in the Study of Vegetation Biochemical properties

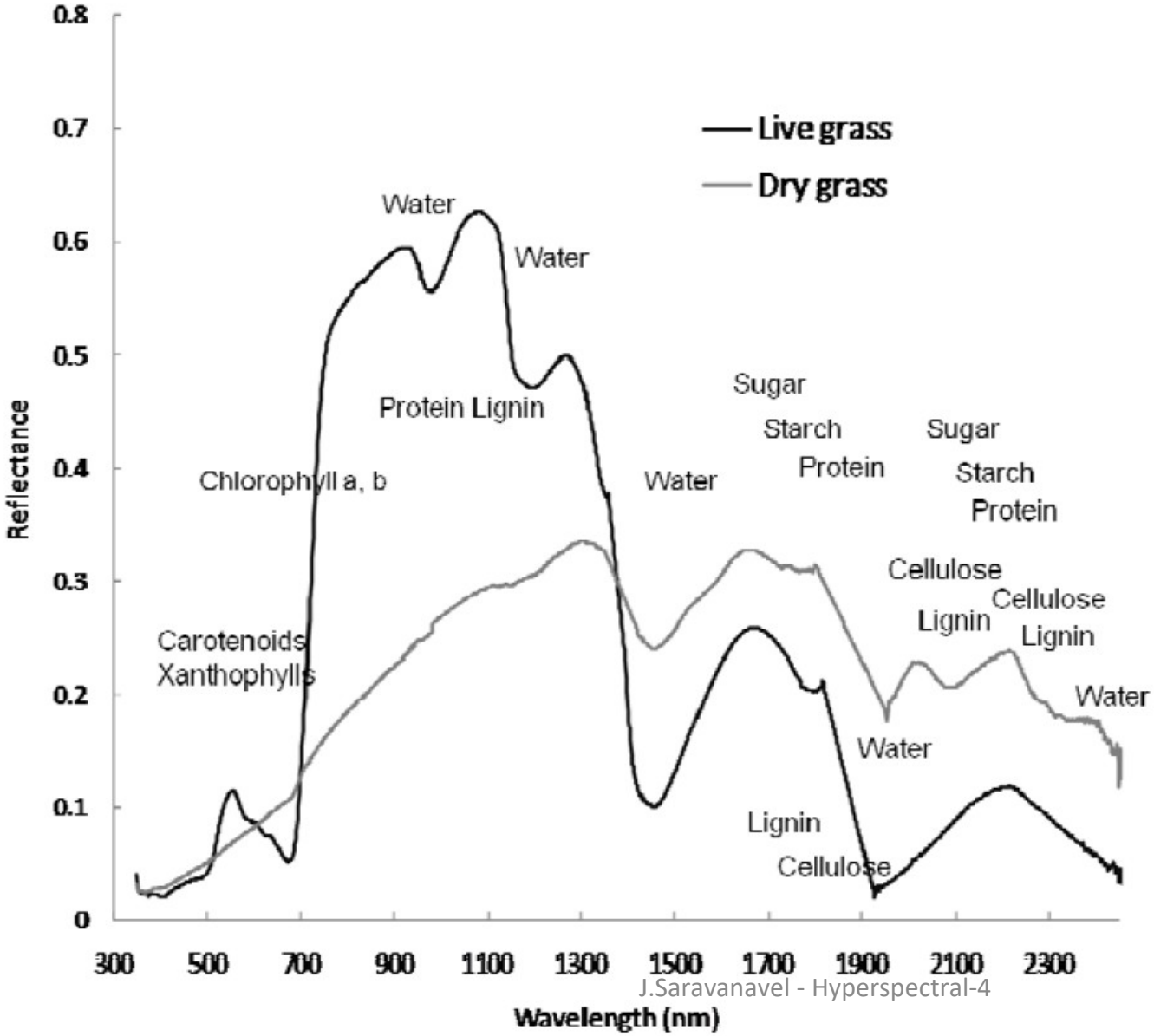

The reflectance spectra with characteristic absorption features associated with plant biochemical constituents for live and dry grass

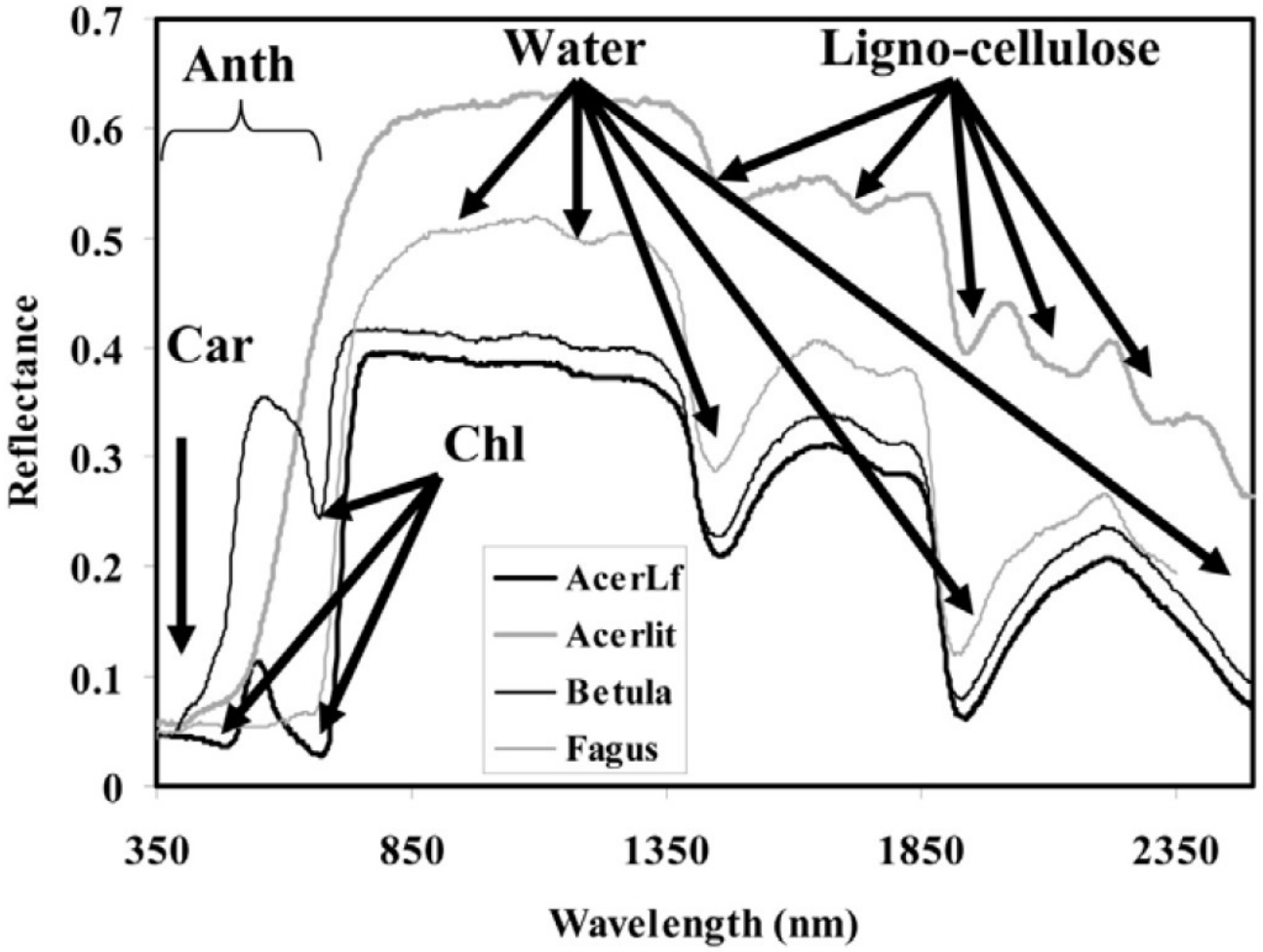

Reflectance spectra of leaves from a senesced birch (Betula), ornamental beech (Fagus) and healthy and fully senesced maple (AcerLf, Acerlit) illustrating Carotenoid (Car), The reflectance spectra with characteristic absorption features associated with plant biochemical constitutents for live and dry grass (Ad t d f Hill [13]) Anthocyanin (Anth), Chlorophyll (Chl), Water and Lignocellulose absorptions

LEAF AREA INDEX

Leaf area index (LAI) is defined as the total area of one-sided green leaves in relationship to the ground below them (FAO 2005; Jensen 2007). Because LAI directly quantifies the vegetation canopy structure, it is highly related to diverse canopy processes, including water interception, photosynthesis, evapotranspiration, and respiration. Thus, LAI information can be used in various terrestrial monitoring and modeling applications to help quantify the processes.

CHLOROPHYLL CONCENTRATION

The chlorophyll concentration in vegetation is mainly responsible for the absorption of photosynthetically active radiation (PAR). A high degree of inter-correlation between canopy photosynthetic rates, LAI, absorbed PAR, and chlorophyll concentrations is normal in natural ecosystems (Boegh et al. 2002; Jensen et al. 1998, 2002). The two optimum spectral regions for sensing the chlorophyll absorption characteristics of a leaf are believed to be in the blue (450 to 520 nm) and red (630 to 690 nm) portions of the spectrum. The former region is characterized by strong absorption by carotenoids and chlorophylls, whereas the latter is characterized by strong chlorophyll absorption (Jensen 2005; Sims and Gamon 2002).

BIOMASS

The amount of dead and live biomass is directly related to the productivity of vegetation (e.g. in agricultural crops). *In situ* biomass measurement generally involves measuring the biomass for various parts of the plant (e.g. root, stem, leaf).

WATER CONTENT

Because water present in the spongy mesophyll of a plant absorbs much of the energy in the mid-infrared spectral region, remote sensing techniques have been used to identify leaf water content. Hence, as the water content of vegetation increases, the reflectance generally decreases in the mid-infrared regions. For example, Figure 5 illustrates how the spectral reflectance of *Bahiagrass* changes according to various irrigation treatments (Garcia-Quijano 2006).

SOIL NUTRIENT AVAILABILITY

The productivity and quality of vegetation are affected by soil nutrient availability, which in turn influences leaf nutrient concentration (Townsend et al. 2003). Leaf nutrients include nitrogen, phosphorus, potassium, calcium, and magnesium. Nitrogen has been explored by many scientists using hyperspectral remote sensing techniques because it is a major nutrient of vegetation. Other nutrients, however, have had relatively less exploration because leaf nutrient levels vary by differences in the physical structure of canopies and there may be no strong linear relationship between spectral signature-derived values and the nutrient levels. Phosphorus and potassium, critical to vegetation growth, are used in various mechanisms, such as fat formation, energy transfer, cell division, and seed sprouting (Jokela et al. 1997; Milton et al. 1991).

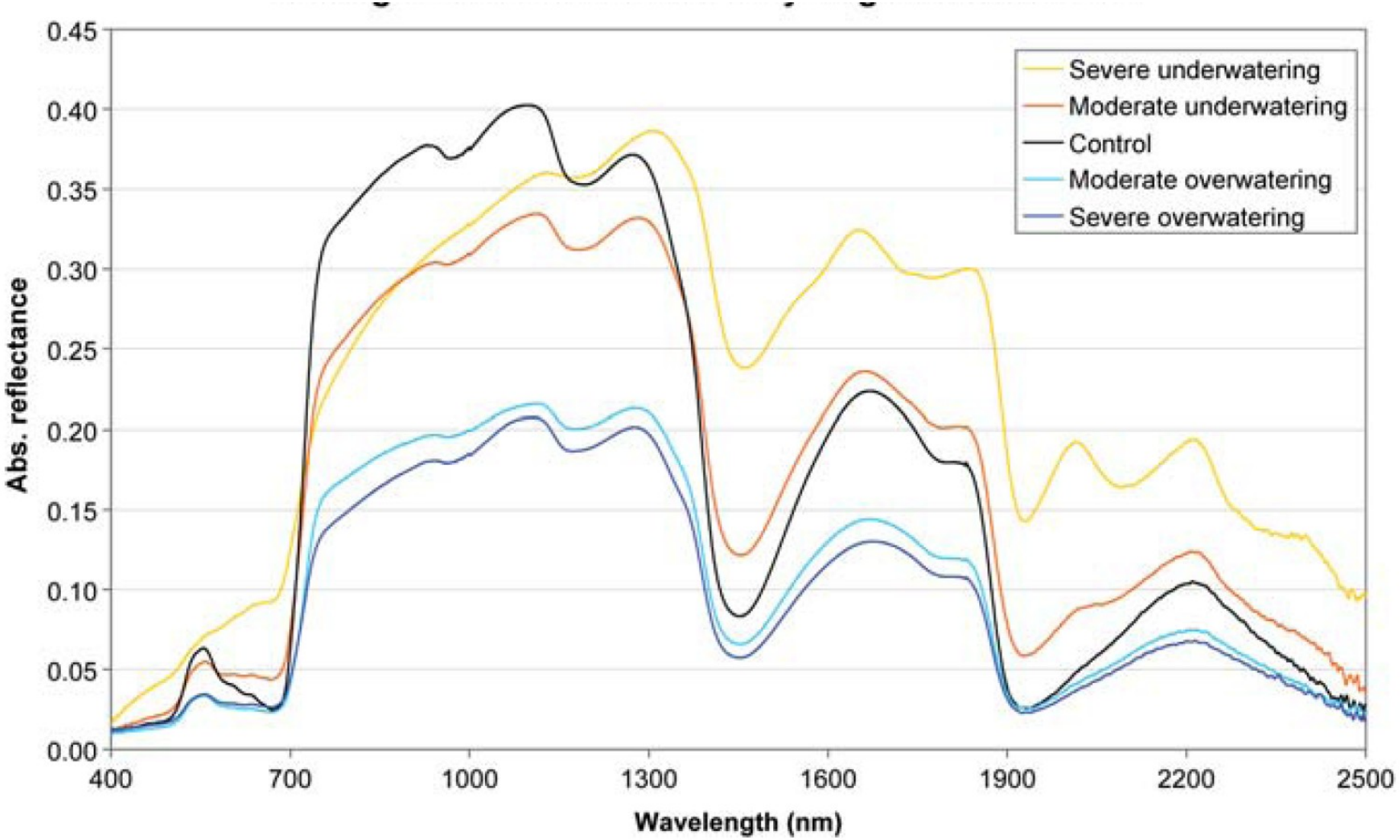

Spectral reflectance curves of Bahiagrass subjected to various irrigation treatments measured using an in situ ASD FieldSpec3 JR spectroradiometer (Garcia-Quijano 2006).

Hyperspectral Remote Sensing of Vegetation

Truck-mounted Hyperspectral sensors

The advantage of airborne, ground-based, and truck-mounted sensors are that they enable relatively cloud free acquisitions that can be acquired on demand anywhere; over the years they have also allowed careful study of spectra in controlled environments to advance the genre.

(a)

(b)

(c)

Truck-mounted Hyperspectral Data Acquisition example

Hyperspectral Data on Tropical Forests

Factors Influencing Spectral Variation over Tropical Forests

1. Biochemistry (e.g., plant pigments, water, and structural carbohydrates): Leaf reflectance in the visible spectrum is dominated by absorption features created by plant pigments, such as:

chlorophyll a (chl-a): absorps in 410-430 nm and 600-690 nm;
chlorophyll b (chl-b): absorps in 450-470 nm;
carotenoids (e.g., β-carotene and lutein): peak absorption in wavebands <500 nm; and
anthocyanins.
Lignin, cellulose, protein, Nitrogen: relatively low reflectance and strong absorption in SWIR bands by water that masks other absorption features

However, dry leaves do not have strong water absorption and reveal overlapping absorptions by carbon compounds, such as lignin and cellulose, and other plant biochemicals, including protein nitrogen,starch, and sugars

Wavelength [nm]	Cause of absorption	Chemicals
430	Electron transition	Chlorophyll a
460	Electron transition	Chlorophyll b
640	Electron transition	Chlorophyll b
660	Electron transition	Chlorophyll a
910	C-H stretch, 3rd overtone	Protein
1020	N-H stretch	Protein
1510	N-H stretch, 1st overtone	Protein, Nitrogen
1690	C-H stretch, 1st overtone	Lignin, Starch, Protein, Nitrogen
1940	O-H stretch, O-H deformation	Water, Lignin, Protein, Nitrogen, Starch, Cellulose
1980	N-H asymmetry	Protein
2060	N-H bend, 2nd overtone / N-H bend / N-H stretch	Protein, Nitrogen
2130	N-H stretch	Protein
2180	N-H bend, 2nd overtone / C-H stretch / C-O stretch C-O stretch / C-N stretch	Protein, Nitrogen
2240	C-H stretch	Protein
2300	N-H stretch / C-H stretch /	Protein, Nitrogen

Knowledge Gain in using Hyperspectral Narrowband Data in Study of Vegetation

2.1a. Thirty-three (33) Optimal Bands in Study of Vegetation

A. Blue bands		
1	405	Nitrogen, Senescing
2	450	Chlorophyll, carotenoids, senescing
3	490	Carotenoid, Light use efficiency (LUE), Stress in vegetation
B. Green bands		
4	515	Pigments (Carotenoid, Chlorophyll, anthocyanins), Nitrogen, Vigor
5	531	Light use efficiency (LUE), Xanophyll cycle, Stress in vegetation, pest and disease
6	550	Anthocyanins, Chlorophyll, LAI, Nitrogen, light use efficiency
7	570	Pigments (Anthrocyanins, Chlorophyll), Nitrogen
C. Red bands		
8	650	Pigment, nitrogen
9	687	Biophysical quantities, chlorophyll, solar induced chlorophyll Floroscense
D. Red-edge bands		
10	705	Stress in vegetation detected in red-edge, stress, drought
11	720	Stress in vegetation detected in red-edge, stress, drought
12	700-740	Chlorophyll, senescing, stress, drought
E. Near infrared (NIR) bands		
13	760	Biomass, LAI, Solar-induced passive emissions
14	855	Biophysical\biochemical quantities, Heavy metal stress
15	970	Water absorption band
16	1045	Biophysical and biochemical quantities

Note 1: Overcomes data redundancy and yet retains optimal solution.

Note 2: for each band, a bandwidth of 3 nm will be ideal, 5 nm maximum to capture the best characteristics of vegetation.

Note:

* = wavebands were selected based on research and discussions in the chapters;

** = when there were close wavebands (e.g., 960 nm, 970 nm), only one waveband (e.g., 970 nm) was selected based on overwhelming eveidence as reported in various chapters. This would avoid redundancy.

*** = a nominal 5 nm waveband width can be considered optimal for obtaining best results with above wavebands as band centers. So, for 970 nm waveband center, we can have a band of range of 968-972 nm.

**** = The above wavebands can be considered as optimal for studying vehetation. Adding more waveband will only add to redundancy. Vegetation indices can be computed using above wavebands.

***** = 33 wavebands lead to a matrix of 33 x 33 = 1089 two band vehetation indices (TBVIs). Given that the indices above the diagonal and below diagonal replicate and indices along diagonal are redundant, there are 5

Knowledge Gain in using Hyperspectral Narrowband Data in Study of Vegetation

2.1b. Thirty-three (336) Optimal Bands in Study of Vegetation

E. Far near infrared (FNIR) bands		
17	1100	Biophysical quantities
18	1180	Water absorption band
19	1245	Water sensitivity
F. Early short-wave infrared (ESWIR) bands		
20	1450	Water absorption band
21	1548	Lignin, cellulose
22	1620	Lignin, cellulose
23	1650	Heavy metal stress, Moisture sensitivity
24	1690	Lignin, cellulose, sugar, starch, protein
25	1760	Water absorption band, senescence, lignin, cellulose
G. Far short-wave infrared (FSWIR) bands		
26	1950	Water absorption band
27	2025	Litter (plant litter), lignin, cellulose
28	2050	Water absorption band
29	2133	Litter (plant litter), lignin, cellulose
30	2145	Water absorption band
31	2173	Water absorption band
32	2205	Litter, lignin, cellulose, sugar, startch, protein; Heavy metal stress
33	2295	Stress and soil iron content

Note 1: Overcomes data redundancy and yet retains optimal solution.

Note 2: for each band, a bandwidth of 3 nm will be ideal, 5 nm maximum to capture the best characteristics of vegetation.

Note:

* = wavebands were selected based on research and discussions in the chapters;

** = when there were close wavebands (e.g., 960 nm, 970 nm), only one waveband (e.g., 970 nm) was selected based on overwhelming eveidence as reported in various chapters. This would avoid redundancy.

*** = a nominal 5 nm waveband width can be considered optimal for obtaining best results with above wavebands as band centers. So, for 970 nm waveband center, we can have a band of range of 968-972 nm.

**** = The above wavebands can be considered as optimal for studying vehetation. Adding more waveband will only add to redundancy. Vegetation indices can be computed using above wavebands.

***** = 33 wavebands lead to a matrix of 33 x 33 = 1089 two band vehetation indices (TBVIs). Given that the indices above the diagonal and below diagonal replicate and indices along diagonal are redundant, there are 5

2. Structure or biophysical (e.g., leaf thickness and air spaces): of leaves, and the scaling of these spectral properties due to volumetric scattering of photons in the canopy;

3. Nonphotosynthetic tissues (e.g., bark, flowers, and seeds); and

4. Other photosynthetic canopy organisms (e.g., vines, epiphytes, and epiphylls) can mix in the photon signal and vary depending on a complex interplay of species, structure, phenology, and site differences

Individual Tree Crown Delineation: Illustrated for 2 species

Figure 19.1

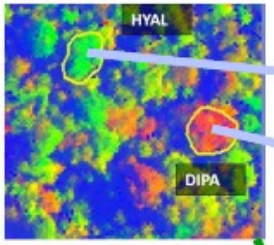

Figure 19.9

Figure. 19.2

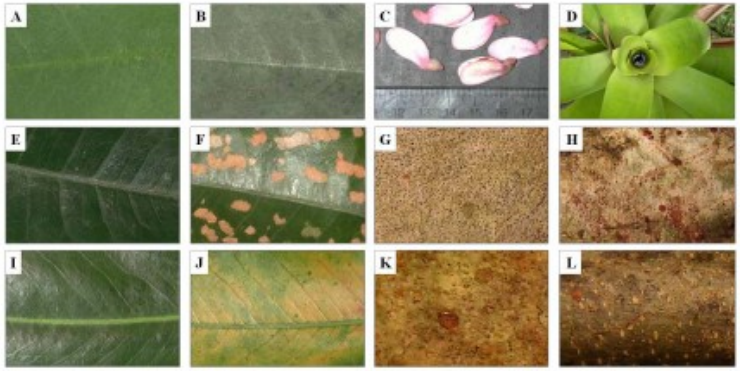

Figure. 19.3

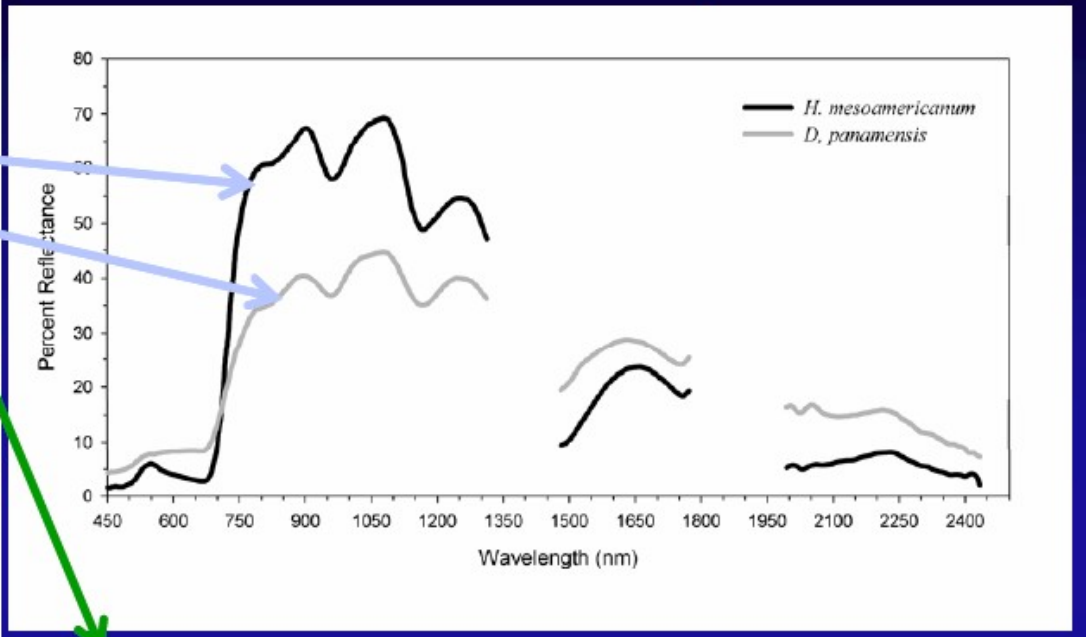

"Fractional abundance of green vegetation (green), non-photosynthetic vegetation (red) and photometric shade (blue) from a spectral mixture analysis.

Individual tree crowns delineated with visual interpretation: *Dipteryx panamensis (DIPA) and Hyeronima alchorneoides (HYAL)."*

Note: see chapter 18, Clark et al.

Hyperspectral Data of Two Dominant Weeds

Chromolaena Odorata in African Rainforests vs. *Imperata Cylindrica* in African Savannas

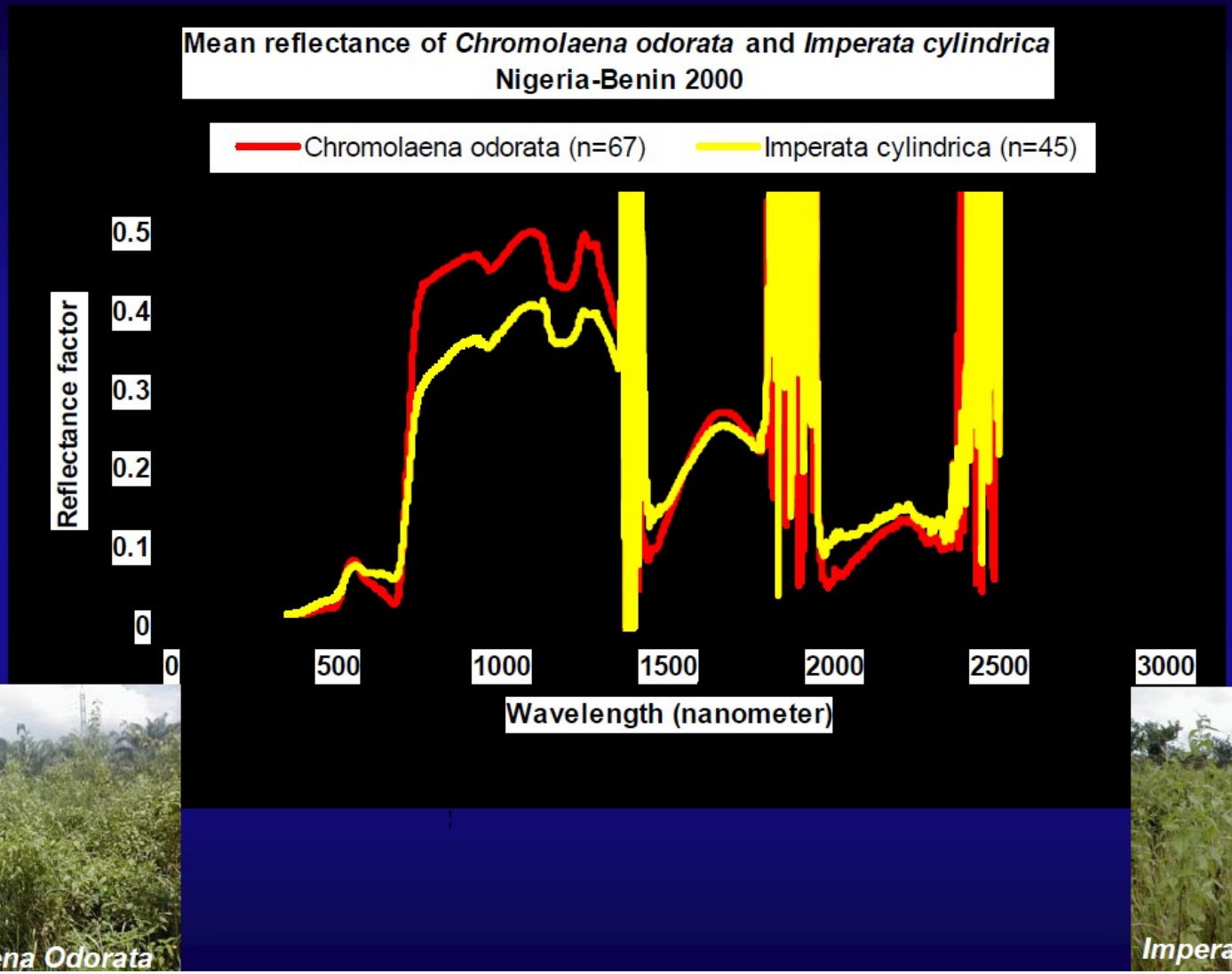

Hyperspectral Data Gathered for the Following Rainforest Vegetation

using Hyperion EO-1 Data and Field-based Measurements of Biophysical Characteristics

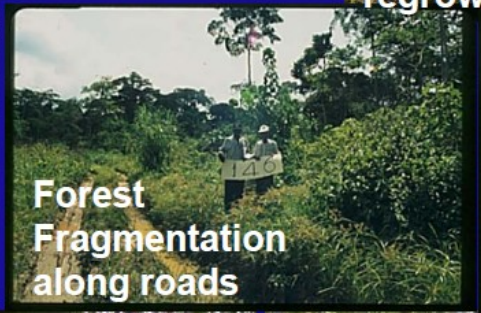

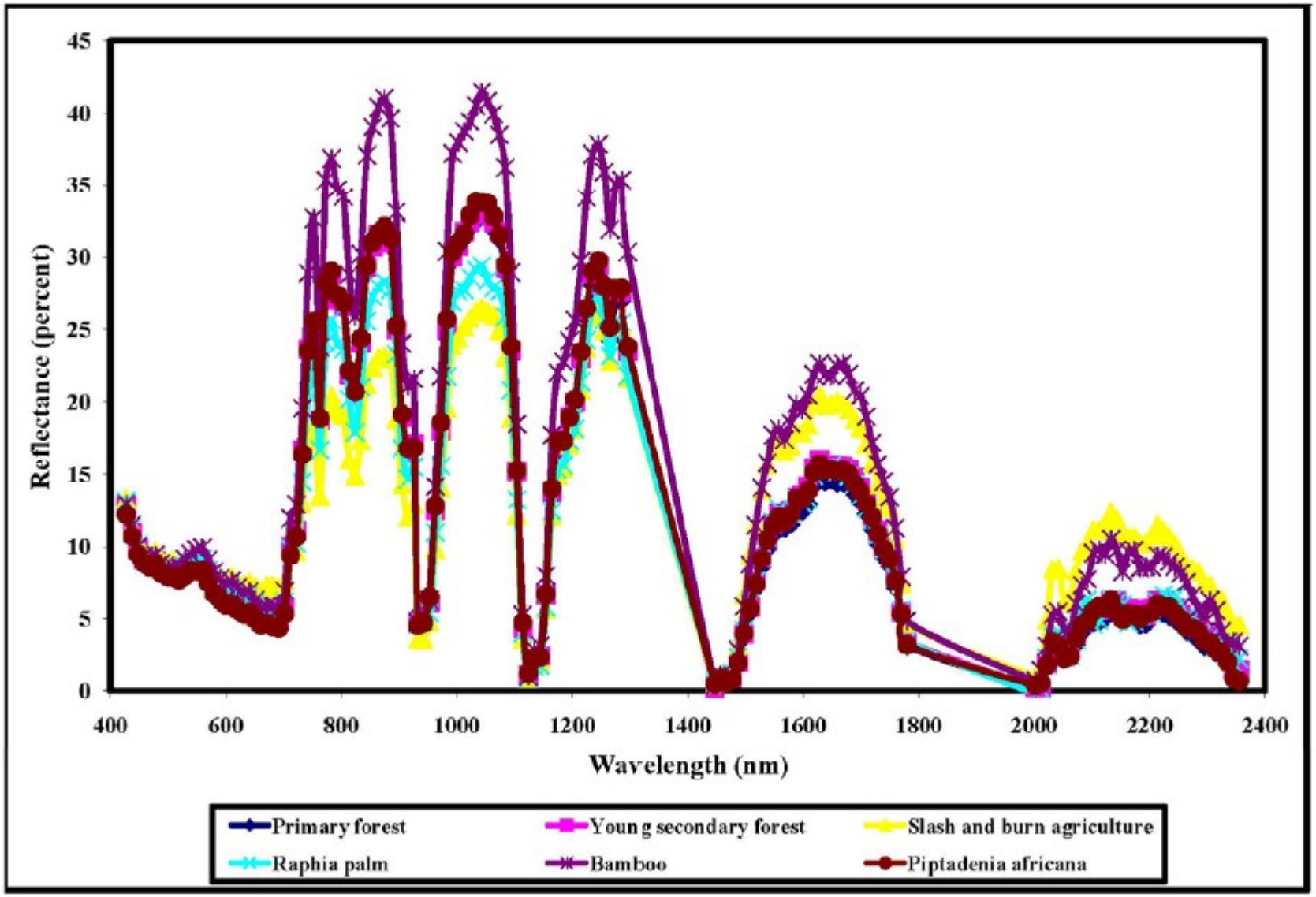
45
40
35
30
25
20
15
10
5
0
Reflectance (percent)
400
600
800
1000
1200
1400
1600
1800
2000
2200
2400
Wavelength (nm)
Primary forest
Young secondary forest
Slash and burn agriculture
Raphia palm
Bamboo
Piptadenia africana

Wheat Crop Versus Barley Crop Versus Fallow Farm

Hyperspectral narrow-band Data for an Erectophile (65 degrees) canopy Structure

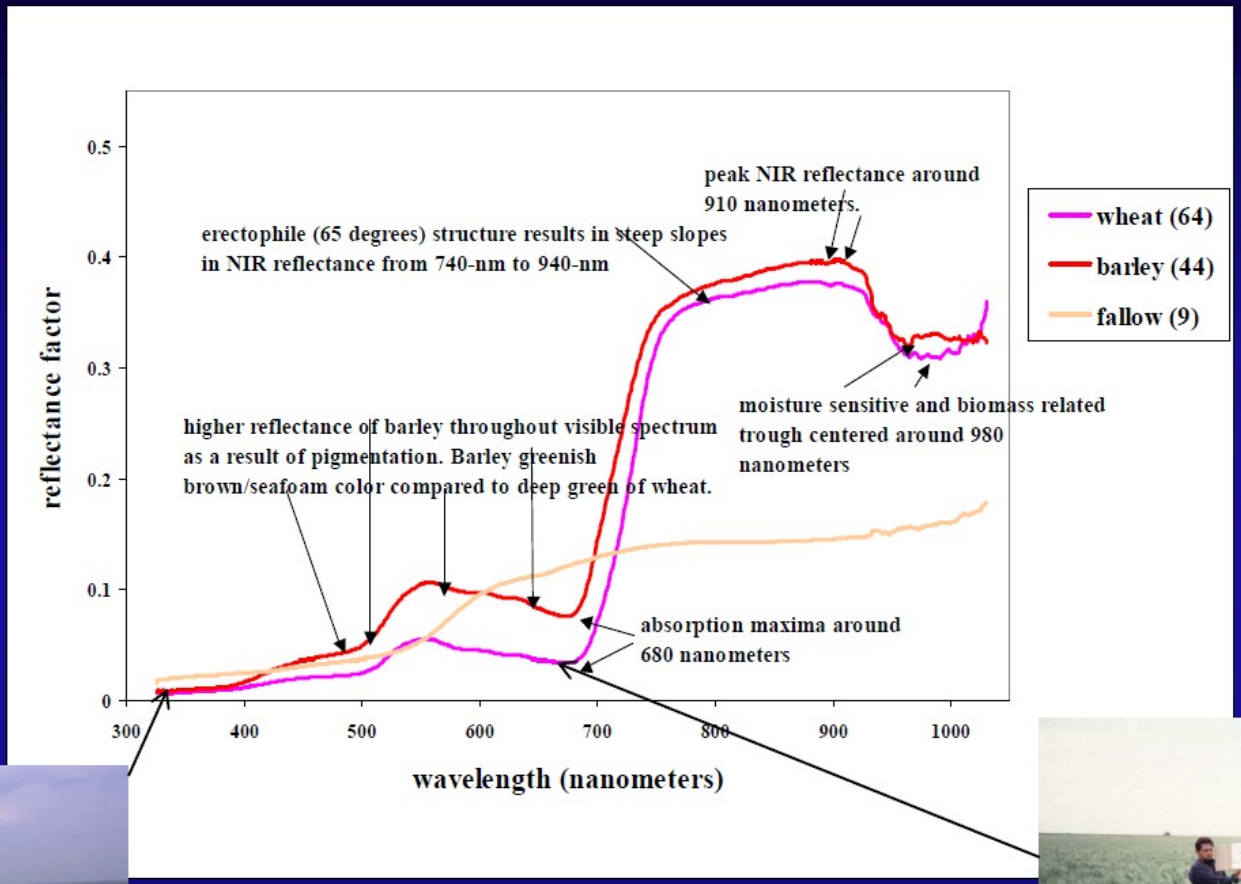

Spectral Wavelengths and their Importance in the Study of Vegetation over Time

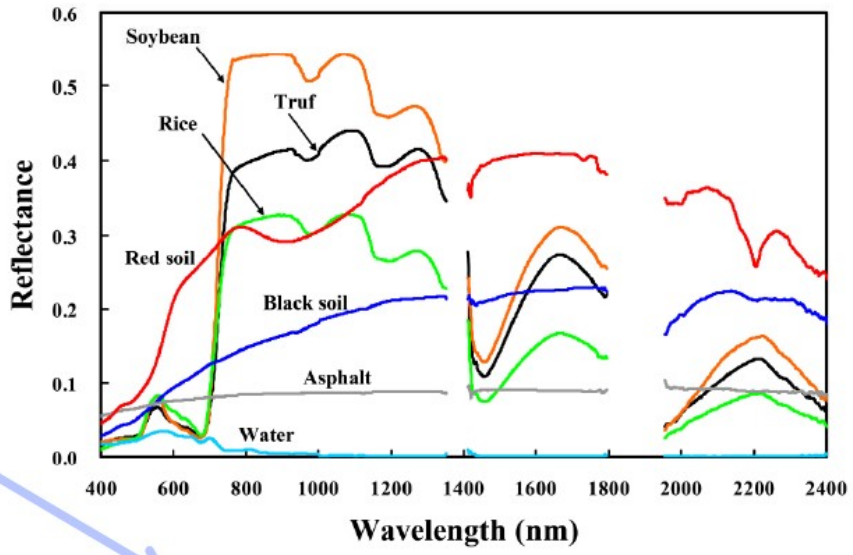

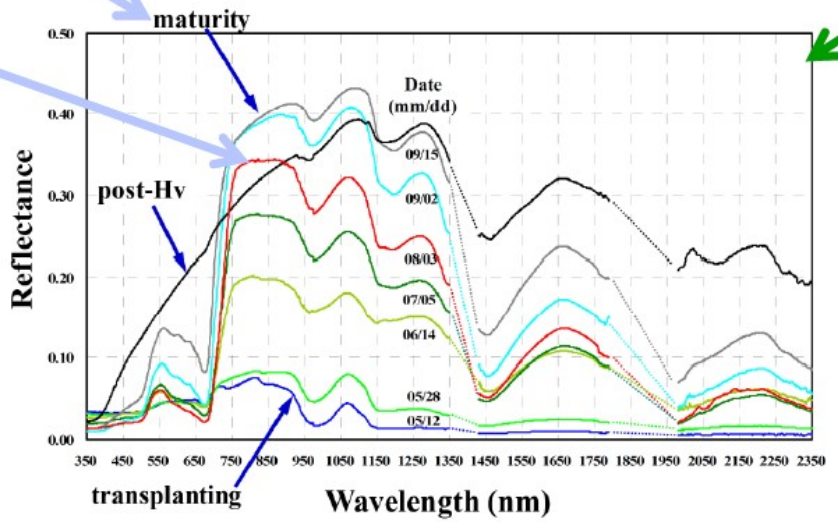

Typical reflectance spectra in agro-ecosystem surfaces (upper), and seasonal changes of spectra in a paddy rice field (lower).

Spectral Wavelengths and their Importance in the Study of Vegetation Stress

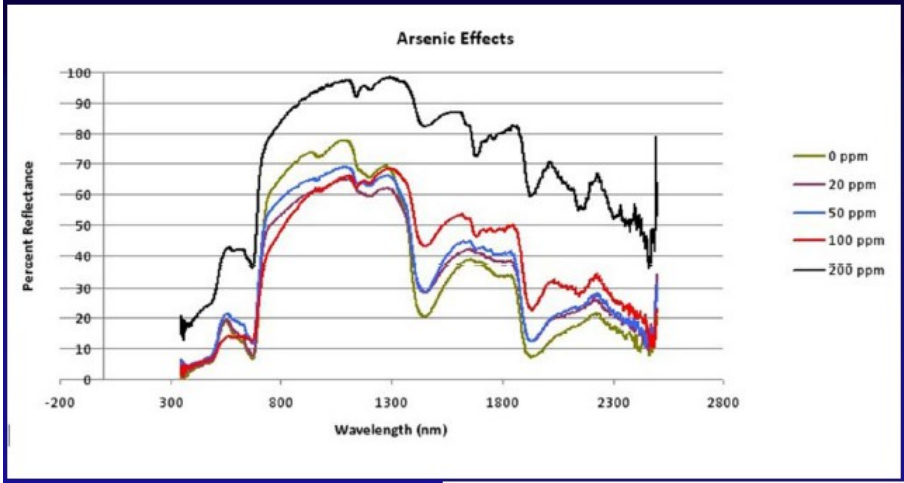

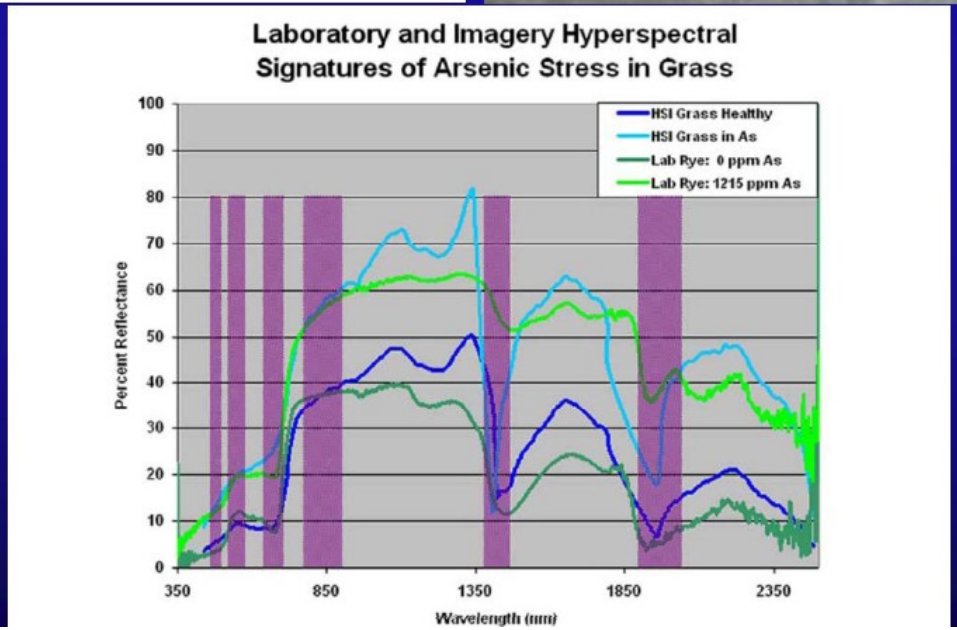

See chapter 23

Spectral Wavelengths and their Importance in the Study of Vegetation in different Growth Stages

Figure 3a. Cotton in critical growth stage.

(a) Cotton (critical)

Figure 3c. Soybeans in critical growth stage.

(b) Soybeans (early)

Figure 3e. Potato in early growth stage.

(c) Potato (early)

Figure 3b. Cotton in yielding/harvest

(a) Cotton (flowering/senescing)

Figure 3d. Soybeans in flowering growth stage.

(b) Soybeans (critical)

Figure 3f. Potato in late growth stage.

(c) Potato (mid-vegetative)

Data was Gathered at Various Growth Stages

Spectral Wavelengths and their Importance in the Study of Vegetation in different Growth Stages

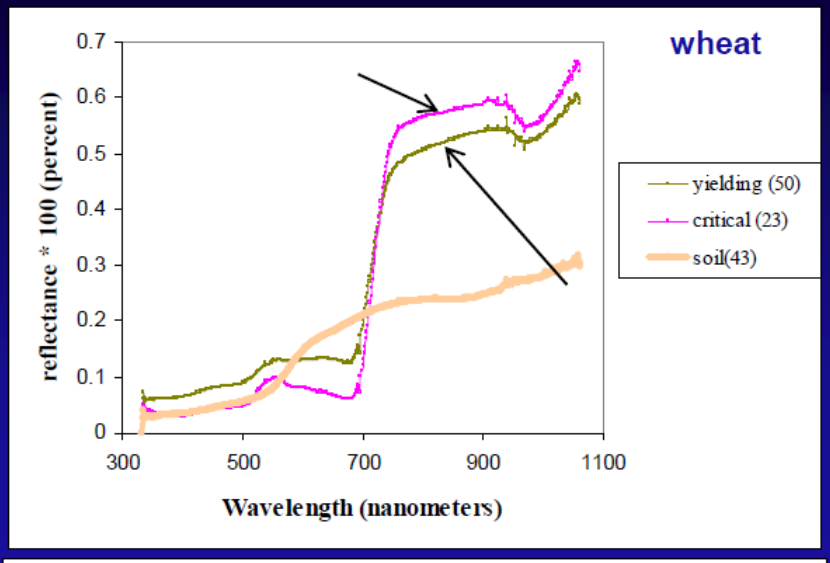

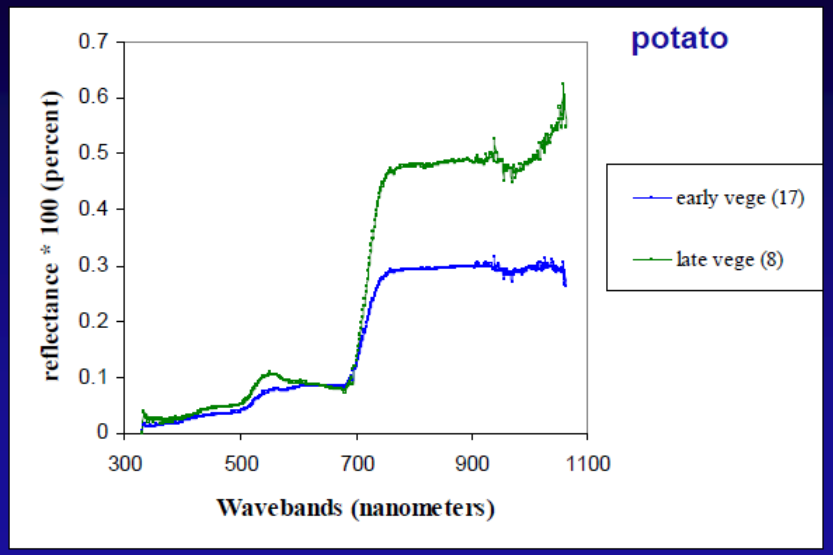

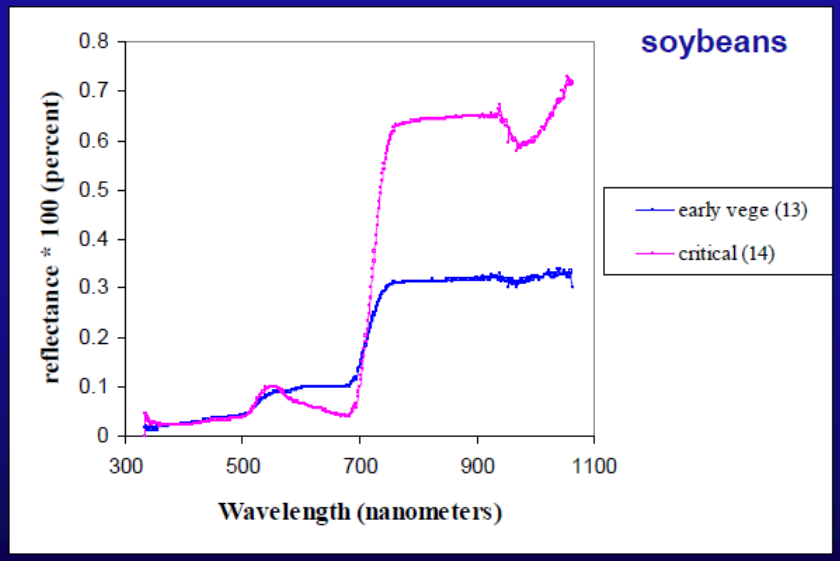

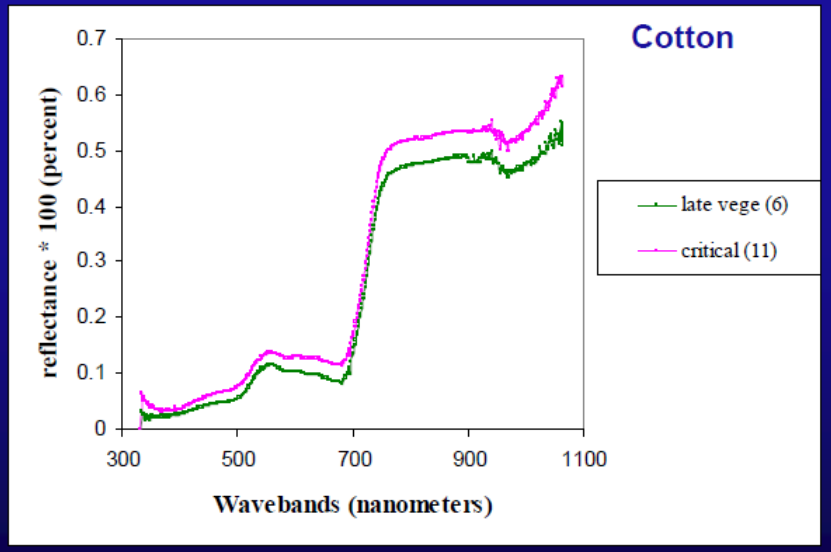

Hyperspectral Vegetation Indices (HVIs)

Table 2. Various vegetation indices used to model vegetation quality and functional health using hyperspectral data (adapted from Jensen 2007).

Vegetation index	Equation	Description	Reference
Near-infrared/red ratio	$Ratio = \frac{\rho_{nir}}{\rho_{red}} = \frac{\rho_{900nm}}{\rho_{660nm}}$	Ratio is highly correlated with vegetation LAI and biomass.	Colombo et al. (2003)
Normalized difference vegetation index (NDVI)	$NDVI = \frac{\rho_{nir} - \rho_{red}}{\rho_{nir} + \rho_{red}} = \frac{\rho_{900nm} - \rho_{660nm}}{\rho_{900nm} + \rho_{660nm}}$	Scientists using hyperspectral data may select among numerous red and NIR hyperspectral bands to use in the NDVI algorithm.	Huete et al. (2002)
MODIS enhanced vegetation index (EVI)	$EVI = G\frac{\rho_{nir} - \rho_{red}}{\rho_{nir} + C_1\rho_{red} - C_2\rho_{blue} + L}(1+L)$ where the coefficients G, C_1, C_2, and L are empirically determined as 2.5, 6.0, 7.5, and 1.0 respectively.	Developed for use with MODIS data. It includes a soil background reflectance factor and corrects for atmospheric aerosol scattering (Jensen 2007).	Huete et al. (2002)
Soil and atmospherically resistant vegetation index (SARVI)	$SARVI = \frac{\rho_{nir} - \rho_{rb}}{\rho_{nir} + \rho_{rb} + L}$ where, $\rho_{rb} = \rho_{red} - \gamma(\rho_{blue} - \rho_{red})$ and γ is normally equal to 1.0 in order to minimize atmospheric effects.	Developed by adding the L function and normalizing the blue band in ARVI. It is less sensitive to noise by soil and atmospheric effects.	Huete and Liu (1994)
Visible atmospherically resistant index (VARI)	$VARI_{green} = \frac{\rho_{green} - \rho_{red}}{\rho_{green} + \rho_{red} - \rho_{blue}} = \frac{\rho_{560nm} - \rho_{660nm}}{\rho_{560nm} + \rho_{660nm} - \rho_{460nm}}$	Less sensitive to atmospheric effects. It is useful when extracting vegetation fraction information over large areas.	Gitelson et al. (2002)
Normalized difference moisture or water index (NDWI)	$NDWI = \frac{\rho_{nir} - \rho_{midIR}}{\rho_{nir} + \rho_{midIR}} = \frac{\rho_{860nm} - \rho_{1240nm}}{\rho_{860nm} + \rho_{1240nm}}$	Useful when extracting vegetation water content information. It was originally based on Landsat TM NIR and middle-infrared bands.	Galvao et al. (2005)
Transformed chlorophyll absorption ratio index/ optimized soil-adjusted vegetation index (TCARI/ OSAVI)	$TCARI = 3\left[\rho_{700} - \rho_{670} - 0.2(\rho_{700} - \rho_{550})\left(\frac{\rho_{700}}{\rho_{670}}\right)\right]$ $OSAVI = \frac{(1+0.16)(\rho_{800} - \rho_{670})}{(\rho_{800} + \rho_{670} + 0.16)}$	Minimizes soil background effects and is sensitive to chlorophyll concentration.	Haboudane et al. (2002)

Hyperspectral Derivative Greenness Vegetation Indices (DGVIs)

First Order Hyperspectral Derivative Greenness Vegetation Index (HDGVI) (Elvidge and Chen, 1995):

These indices are integrated across the (a) chlorophyll red edge:.626-795 nm, (b) Red-edge more appropriately 690-740 nm……and other wavelengths.

$$DGVI1 = \sum_{\lambda_1}^{\lambda_n} \frac{(\rho'(\lambda_i) - (\rho'(\lambda j)}{\Delta\lambda_I}$$

Where, I and j are band numbers,

λ = center of wavelength,

λ_1 = 0.626 μm,

λ_n = 0.795 μm,

ρ' = first derivative reflectance.

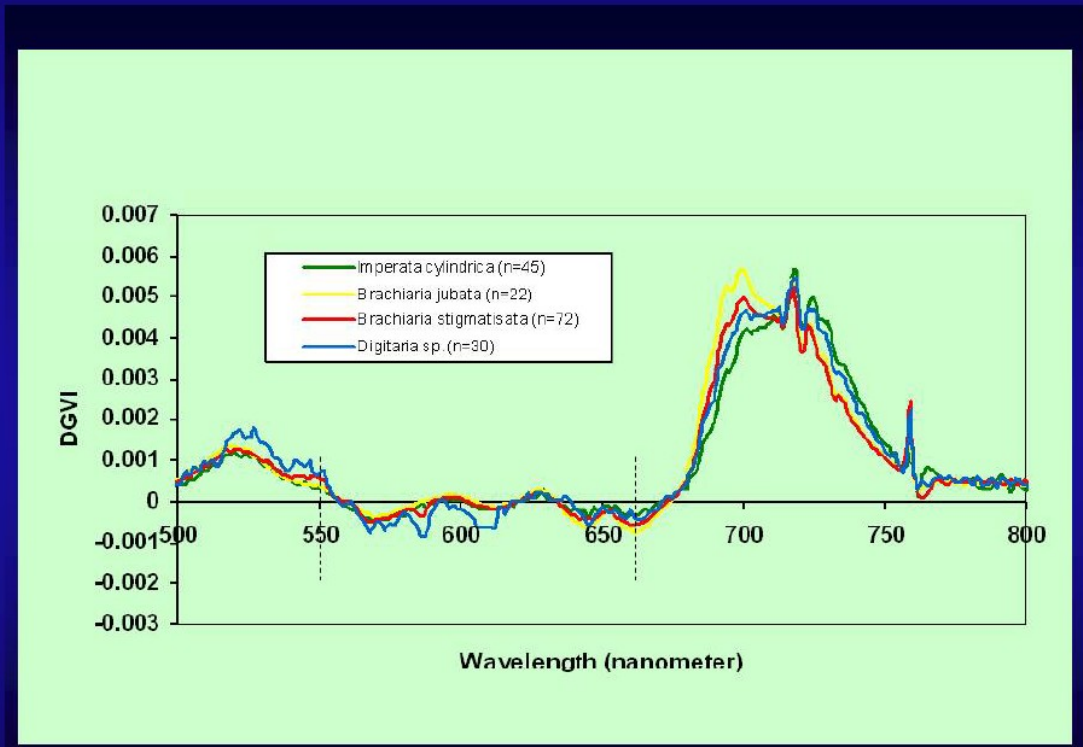

Note: HDGVIs are near-continuous narrow-band spectra integrated over certain wavelengths

Hyperspectral Derivative Greenness Vegetation Indices (DGVIs) vs. Forest Biomass

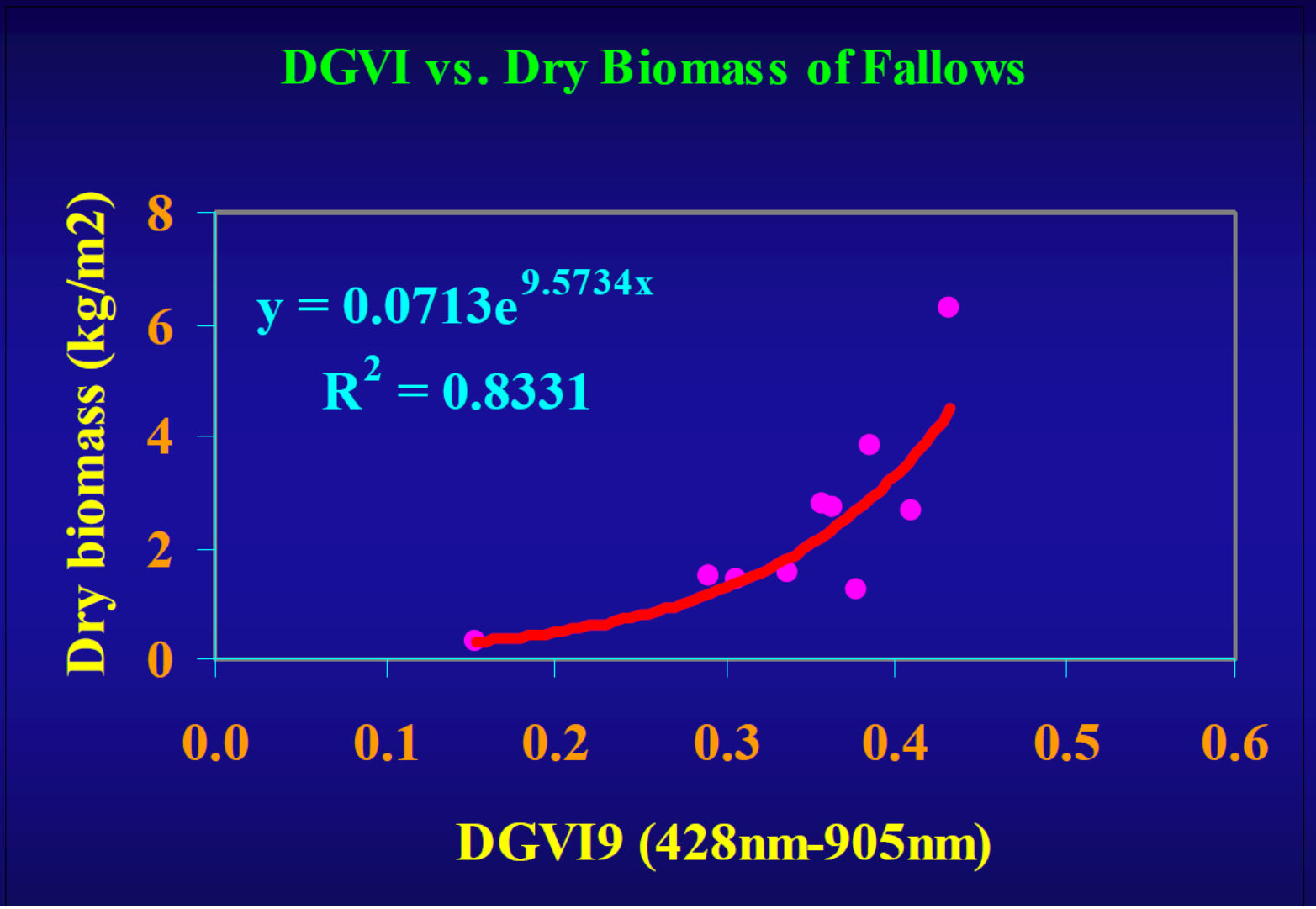

HVIs: Biophysical, Biochemical, Pigment, Water, Lignin and cellulose, and Physiology

Index	Equation	Reference
Structure (LAI, green biomass, fraction)		
*NDVI	$(R_{NIR}-R_{red})/(R_{NIR}+R_{red})$	Rouse et al.[15]
*SR	R_{NIR}/R_{red}	Jordan [3]
*EVI	$2.5*(R_{NIR}-R_{red})/(R_{NIR}+6*R_{red}-7.5*R_{blue}+1)$	Huete et al.[23]
*NDWI	$(R_{857}-R_{1241})/(R_{857}+R_{1241})$	Gao [29]
**WBI	R_{900}/R_{970}	Peñuelas et al.[28]
*ARVI	$(R_{NIR}-[R_{red}-\gamma*(R_{blue}-R_{red})])/(R_{NIR}+[R_{red}-\gamma*(R_{blue}-R_{red})])$	Kaufman & Tanré [22]
*SAVI	$[(R_{NIR}-R_{red})/(R_{NIR}+R_{red}+L)]*(1+L)$	Huete [21]
**1DL_DGVI	$\sum_{\lambda_{626\ nm}}^{\lambda_{795\ nm}} \lvert R'(\lambda_i) - R'(\lambda_{626\ nm})\rvert \Delta\lambda_i$	Elvidge & Chen [1]
**1DZ_DGVI	$\sum_{\lambda_{626\ nm}}^{\lambda_{795\ nm}} \lvert R'(\lambda_i)\rvert \Delta\lambda_i$	Elvidge & Chen [1]
*VARI	$(R_{green}-R_{red})/(R_{green}+R_{red}-R_{blue})$	Gitelson et al.[13]
*VIgreen	$(R_{green}-R_{red})/(R_{green}+R_{red})$	Gitelson et al.[13]
Biochemical		
Pigments		
**SIPI	$(R_{800}-R_{445})/(R_{800}-R_{680})$	Peñuelas et al. [31]
**PSSR	(R_{800}/R_{675}); (R_{800}/R_{650})	Blackburn [30]
**PSND	$[(R_{800}-R_{675})/(R_{800}+R_{675})]$; $[(R_{800}-R_{650})/(R_{800}+R_{650})]$	Blackburn [32]
**PSRI	$(R_{680}-R_{500})/R_{750}$	Merzlyak et al. [33]
Chlorophyll		
**CARI	$[(R_{700}-R_{670})-0.2*(R_{700}-R_{550})]$	Kim [34]
**MCARI	$[(R_{700}-R_{670})-0.2*(R_{700}-R_{550})]*(R_{700}/R_{670})$	Daughtry et al. [35]
**$CI_{red\ edge}$	$R_{NIR}/R_{red\ edge}-1$	Gitelson et al. [36]
Anthocyanins		
**ARI	$(1/R_{green})-(1/R_{red\ edge})$	Gitelson et al.[40]
**mARI	$[(1/R_{green})-(1/R_{red\ edge})]*R_{NIR}$	Gitelson et al. [36]
**RGRI	R_{red}/R_{green}	Gamon & Surfus [7]
**ACI	R_{green}/R_{NIR}	Van den Berg & Perkins [41]
Carotenoids		
**CRI1	$(1/R_{510})-(1/R_{550})$	Gitelson et al.[42]
**CRI2	$(1/R_{510})-(1/R_{700})$	Gitelson et al. [42]
Water		
*NDII	$(R_{NIR}-R_{SWIR})/(R_{NIR}+R_{SWIR})$	Hunt & Rock [12]
*NDWI, **WBI	See Above	See Above
*MSI	R_{SWIR}/R_{NIR}	Rock et al. [43]
Lignin &Cellulose/Residues		
**CAI	100*[0.5*(R2031+R2211)-R2101]	Daughtry [47]
**NDLI	$[\log(1/R_{1754})-\log(1/R_{1680})]/[\log(1/R_{1754})+\log(1/R_{1680})]$	Serrano et al. [48]
Nitrogen		
**NDNI	$[\log(1/R_{1510})-\log(1/R_{1680})]/[\log(1/R_{1510})+\log(1/R_{1680})]$	Serrano et al. [48]
Physiology		
Light Use Efficiency		
RGRI,SIPI	See Above	See Above
**PRI	$(R_{530}-R_{570})/(R_{530}+R_{570})$	Gamon et al. [9]
Stress		
*MSI	See Above	See Above
**REP	l(max first derivitive: 680-750 nm)	Horler et al. [10]
**RVSI	$[(R_{714}+R_{752})/2-R_{733}$	Merton & Huntington [52]

HVIs: Biophysical, Biochemical, Pigment, Water, Lignin and cellulose, and Physiology

Spectral index	Characteristics & functions	Definition	Reference
Multiple bioparameters:			
LI, Lepidium Index	To be sensitive to the uniformly bright reflectance displayed by *Lepidium* in the visible range.	R_{630}/R_{586}	[20]
NDVI, Normalized Difference Vegetation Index	Respond to change in the amount of green biomass and more efficiently in vegetation with low to moderate density.	$(R_{NIR}-R_R)/(R_{NIR}+R_R)$	[74]
PSND, Pigment-Specific Normalized Difference	Estimate LAI and carotenoids (Cars) at leaf or canopy level	$(R_{800}-R_{470})/(R_{800}+R_{470})$	[74]
SR, Simple Ratio	Same as **NDVI**	R_{NIR}/R_R	[76,77]
Pigments:			
Chl_{green}, Chlorophyll Index Using Green Reflectance	Estimate chlorophylls (Chls) content in anthocyanin-free leaves if NIR is set	$(R_{760-800}/R_{540-560})-1$	[78]
$Chl_{red-edge}$, Chlorophyll Index Using Red Edge Reflectance	Estimate Chls content in anthocyanin-free leaves if NIR is set	$(R_{760-800}/R_{690-720})-1$	[78]
LCI, Leaf Chlorophyll Index	Estimate Chl content in higher plants, sensitive to variation in reflectance caused by Chl absorption	$(R_{850}-R_{710})/(R_{850}+R_{680})$	[79]
mND_{680}, Modified Normalized Difference	Quantify Chl content and sensitive to low content at leaf level.	$(R_{800}-R_{680})/(R_{800}+R_{680}-2R_{445})$	[80]
mND_{705}, Modified Normalized Difference	Quantify Chl content and sensitive to low content at leaf level. **mND_{705}** performance better than **mND_{680}**	$(R_{750}-R_{705})/(R_{750}+R_{705}-2R_{445})$	[80,81]
mSR_{705}, Modified Simple Ratio	Quantify Chl content and sensitive to low content at leaf level.	$(R_{750}-R_{445})/(R_{705}-R_{445})$	[80]

HVIs: Biophysical, Biochemical, Pigment, Water, Lignin and cellulose, and Physiology

mSR_{705}, Modified Simple Ratio	Quantify Chl content and sensitive to low content at leaf level.	$(R_{750}-R_{445})/(R_{705}-R_{445})$	[80]
NPCI, Normalized Pigment Chlorophyll ratio Index	Assess Cars/Chl ratio at leaf level	$(R_{680}-R_{430})/(R_{680}+R_{430})$	[82]
PBI, Plant Biochemical Index	Retrieve leaf total Chl and nitrogen concentrations from satellite hyperspectral data	R_{810}/R_{560}	[83]
PRI, Photochemical / Physiological Reflectance Index	Estimate Car pigment contents in foliage	$(R_{531}-R_{570})/(R_{531}+R_{570})$	[84]
PI2, Pigment index 2	Estimate pigment content in foliage	R_{695}/R_{760}	[85]
RGR, Red:Green Ratio	Estimate anthocyanin content with a green and a red band	R_{683}/R_{510}	[80,86]
SGR, Summed Green Reflectance	Quantify Chl content	Sum of reflectances from 500 to 599 nm	[81]
Floliar chemistry:			
CAI, Cellulose Absorption Index	Cellulose & lignin absorption features, discriminates plant litter from soils	$0.5(R_{2020}+R_{2220})-R_{2100}$	[87]
NDLI, Normalized Difference Lignin Index	Quantify variation of canopy lignin concentration in native shrub vegetation	$[\log(1/R_{1754})-\log(1/R_{1680})]$ / $[\log(1/R_{1754})+\log(1/R_{1680})]$	[88]
NDWI, ND Water Index	Improving the accuracy in retrieving the vegetation water content at both leaf and canopy levels	$(R_{860}-R_{1240})/(R_{860}+R_{1240})$	[89,90]
RVI_{hyp}, Hyperspectral Ratio VI	Quantify LAI and water content at canopy level.	R_{1088}/R_{1148}	[91]
WI, Water Index	Quantify relative water content at leaf level	R_{900}/R_{970}	[92]

Study of Pigments: chlorophyll

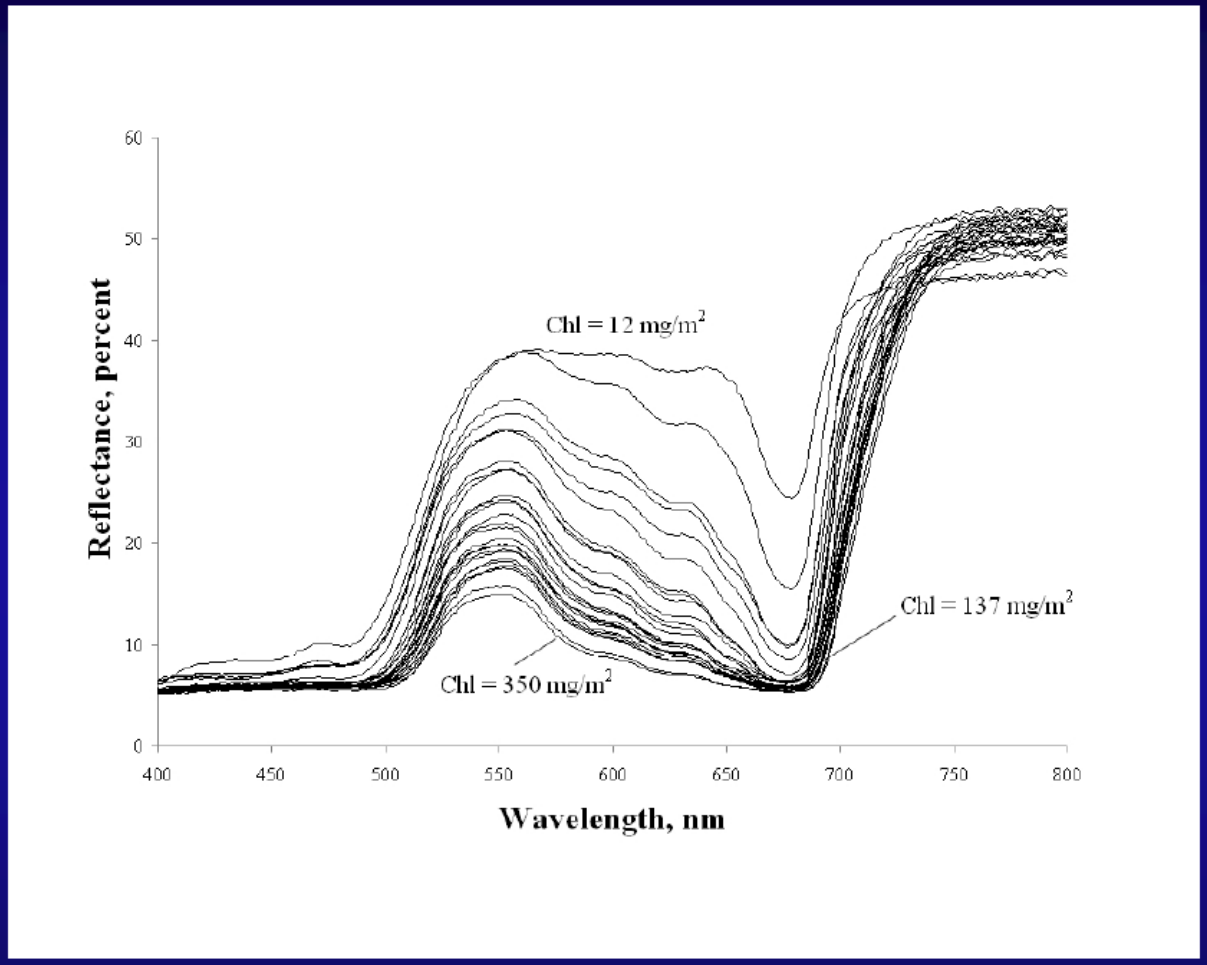

e.g., Reflectance spectra of beech leaves…red-edge (700-740 nm) one of the best.

Study of Pigments: carotenoids/chlorophyll

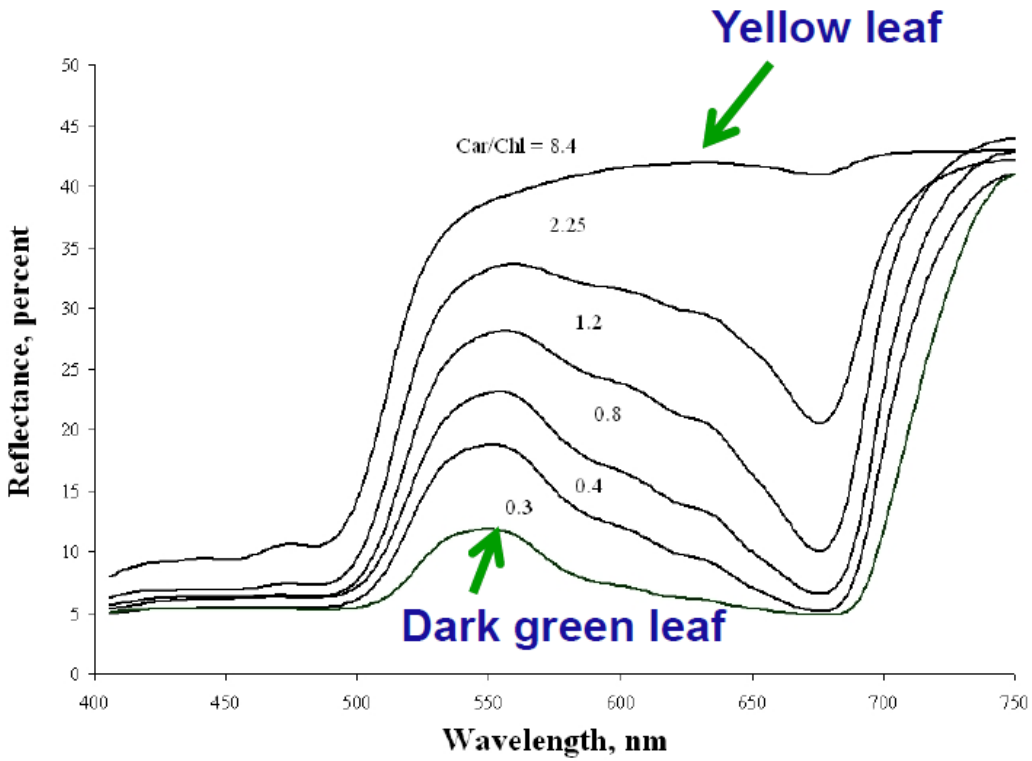

e.g., Reflectance spectra of chestnut leaves…difference reflectance of (680-500 nm)/750 nm quantitative measurement of plant senescence

Hyperspectral Remote Sensing in SOIL

Soil is a complex system with highly variable in physical and chemical properties (Ben-Dor et al., 1999). Both chemical and physical properties have spectral responses and affect the shape and nature of a soil spectrum.

Raw data, first-, and second-derivatives each provide valuable information that can be analyzed separately or combined using multivariate statistical methods or data mining techniques. Soil constituents have unique absorption features in these wavelength regions due to overtones related to stretching and bending vibrations in molecular bonds such as C–C, C–H, N–H and O–H (Dalal and Henry, 1986).

This comprises the physical basis for the application of remote sensing to map soil properties. Soil chemical chromophores (specific absorption of spectrally active group) are materials in a soil system that absorb incident radiation in discreet energy levels.

Soil has three major chemical chromophores: mineral (mostly clay and iron oxides), organic matter and water (Ben-Dor, 2002).

The spectral features of clay minerals are associated with oventones and combination modes of fundamental vibrations of functional groups in the infrared region.

In general, three major spectral regions are active for clay: 1.3 - 1.4, 1.8 - 1.9, and 2.2 - 2.5 µm (Ben-Dor, 2002).

This is mainly based on specific absorption of spectrally active groups such as Fe, OH- in water and minerals, CO3, Al, (Mg) OH, SO4 in minerals, and any others in organic matter.

Iron oxides can change soil color significantly due to selective light absorption in the visible range. Soil iron content is highly correlated with the absorbance in the spectral region 0.6 to 1.0 µm.

Soil organic matter (SOM) consists of plant and animal residues in different stages of decomposition. SOM has strong influence on soil reflectance, absorbing light through the VIS-NIR-SWIR (visible-near infrared-shortwave infrared) region.

Ben-Dor et al. (1997) observed decreased soil albedo across the VIS-NIR-SWIR region as the organic matter aged.

They suggested that the reflectance slope between 450 and 638 nm may be useful for identifying both the degradation condition and the parent material status of the organic matter and the reflectance slope between 680 and 800 nm may be used as a general parameter for monitoring organic matter maturity.

Moreover, organic matter was found to be correlated with the spectral region 0.5 to 1.2 µm (Mathews et al., 1973) and that the region 0.9 to 1.22 µm is good for mapping soil organic matter (Beck et al., 1976).

Three major forms of water exist in soil: hydration water incorporated into the lattice of the minerals, hygroscopic water adsorbed on soil surface areas as a thin layer and free water filling soil pores (Ben-Dor, 2002).

Like SOM, moisture decreases soil reflectance in the VIS-NIR-SWIR region. Spectra of a mixed system of water and minerals, exhibit OH absorption features at around 0.95 µm (very weak), 1.2 µm (weak), 1.4 µm (strong) and 1.9 µm (very strong).

soil properties can be estimated from spectra of moisture free soil more accurately than those of moist soil.

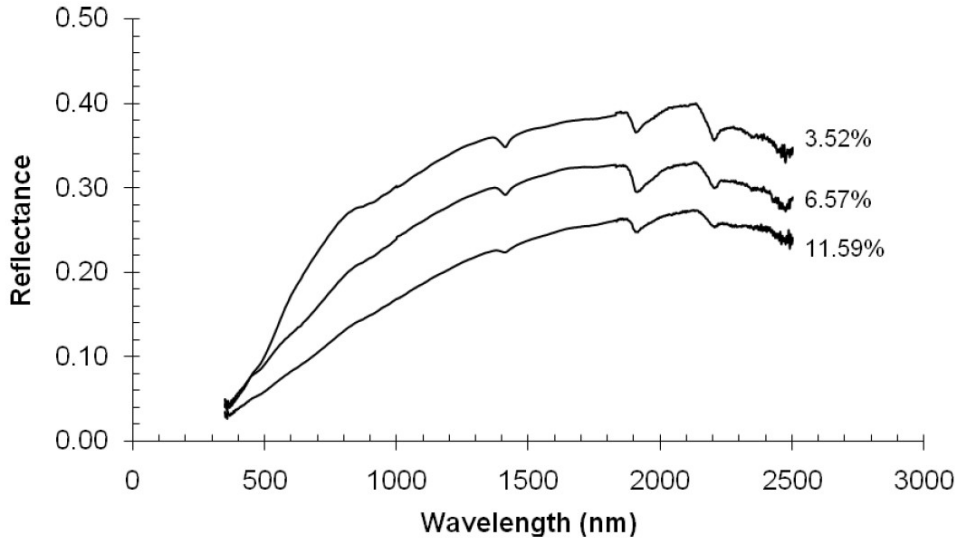

Spectra of oven-dried soil with different content of organic matter (A); Moisture effect on reflectance spectra of soils with similar amounts of organic matter and different moisture content (B)

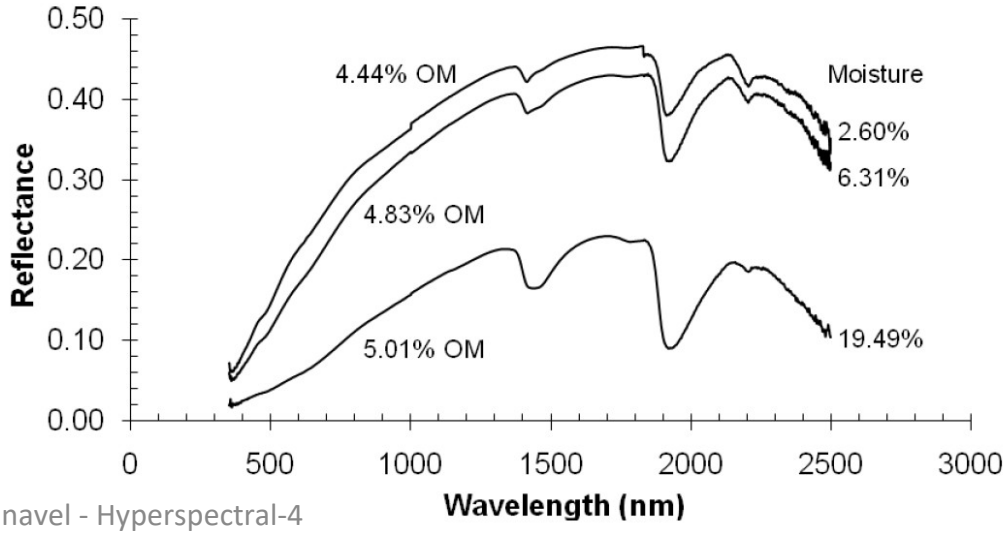

Spectral response pattern of soil is generally governed by a number of factors. The properties of soils that govern their spectral reflectance are colour, texture, structure, mineralogy, organic matter, free carbonates, salinity, moisture and the oxides/ hydroxides of iron and manganese.

Chemical compositions of the soil influences spectral signature of soils through the absorption processes. In near infrared (NIR) and middle infrared (MIR) domain, absorption feature of soil components in solid phase originate primarily from the vibrations of bounded nuclei.

In addition to vibrations, molecular rotation and transition may occur in the pores where gas and water molecules reside, which also results in higher absorption in MIR region. Soil water exhibits absorption peaks at about 1450 nm, 1880 nm and 2660 nm (Hoffer 1978).

Table 1. Summary of vibrational features (Source: Bear 1968).

Constituents/Modes	Reactions	Absorption wavelength (nm)
H^2O	- Symmetric stretch	3106
	- Asymmetric stretch	2903
	- H-O-H bend	6080
	Stretching fundamental	2770
	A1-or Mg-OH bend	2200 or 2300
Oxides	- Fundamental stretching	5000
Hematite	- Fe-O fundamental stretching	20000
Carbonates		7000, 11000-12000
		13000-15000
Phosphates		9250, 10300,18000
		28500
Sulphates		9000, 10, 200, 16000, 22200
Gypsum	- Overtones and combination of OH stretching in molecular water	1750, 2300
	- Fundamental bending mode of constitutional water	6000
	- Si-O bending	around 5000
Silicates	- Si-O stretching	1000
	- Si-O-Si, A1-O-Si stretches	12000-15000
	- (Si, A1)-O-(A1, Si) stretch	15000-20000
	- Deformation and bending modes of O-(Al, Si)-O, (Si, A1)-O-(Si, A1) O-(A1,Si)-O	20000-40000
	- A1, Si-O metal valence stretching	20000-40000

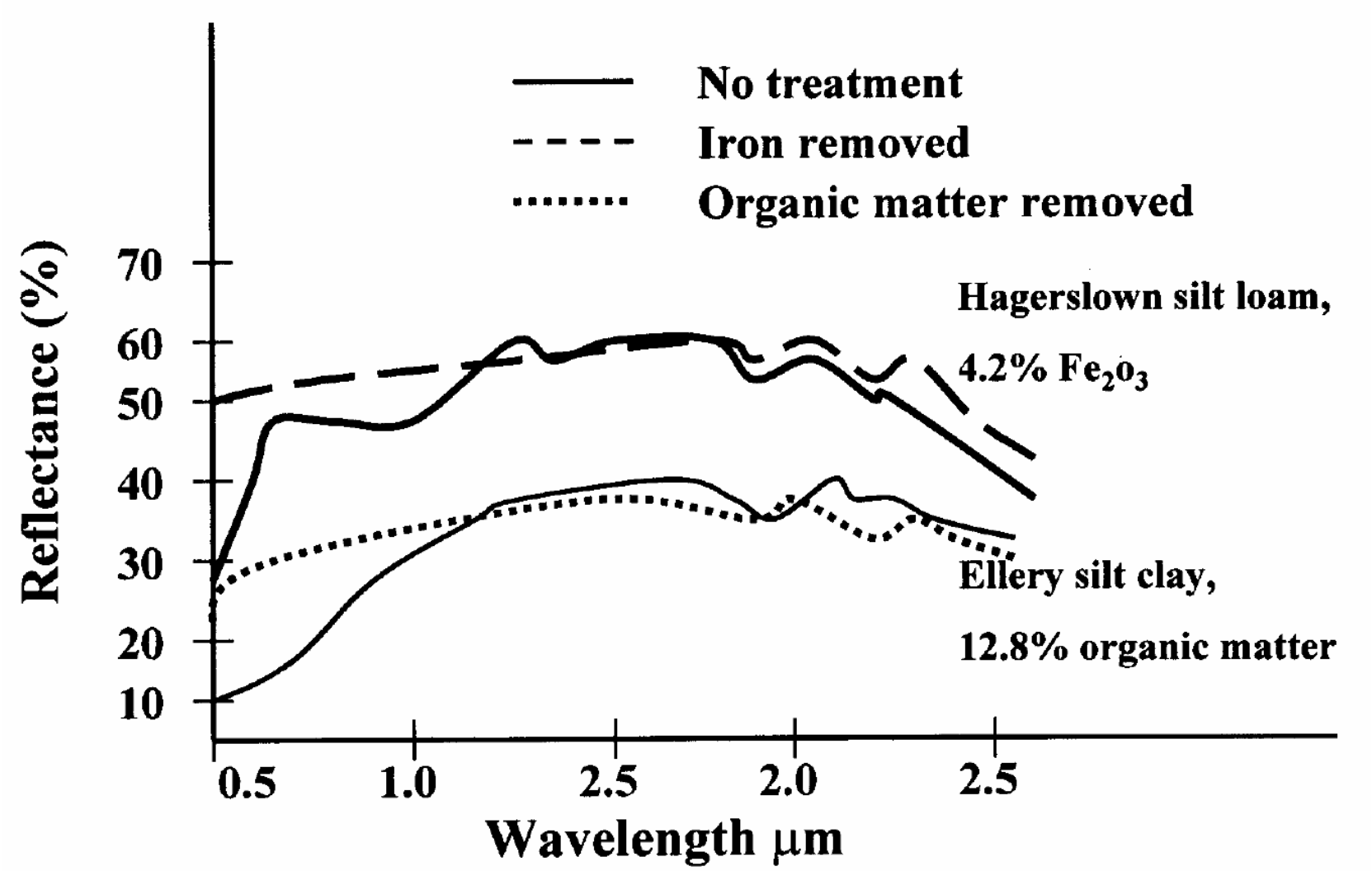
No treatment
Iron removed
Organic matter removed
Reflectance (%)
70
60
50
40
30
20
10
Hagerslown silt loam,
4.2% Fe_2o_3
Ellery silt clay,
12.8% organic matter
0.5
1.0
2.5
2.0
2.5
Wavelength μm

Electronic transition processes require much higher energy levels which causes absorption of light at lower wavelengths. Transition elements (Fe, Mn, Ti etc.) explain most of the decrease in reflectance observed towards the lower wavelength spectral domain (Hunt & Salisbury 1976; Hunt 1980).

Organic matter absorbs strongly in shorter wavelength as well as in the infrared region due to the presence of various functional groups and conjugate bonds (Hoffer 1978; Hunt 1980).

Soil texture refers to relative proportion of sand, silt & clay and affects the spectral reflectance of the soils due to its influence on water holding capacity and the size of soil particles.

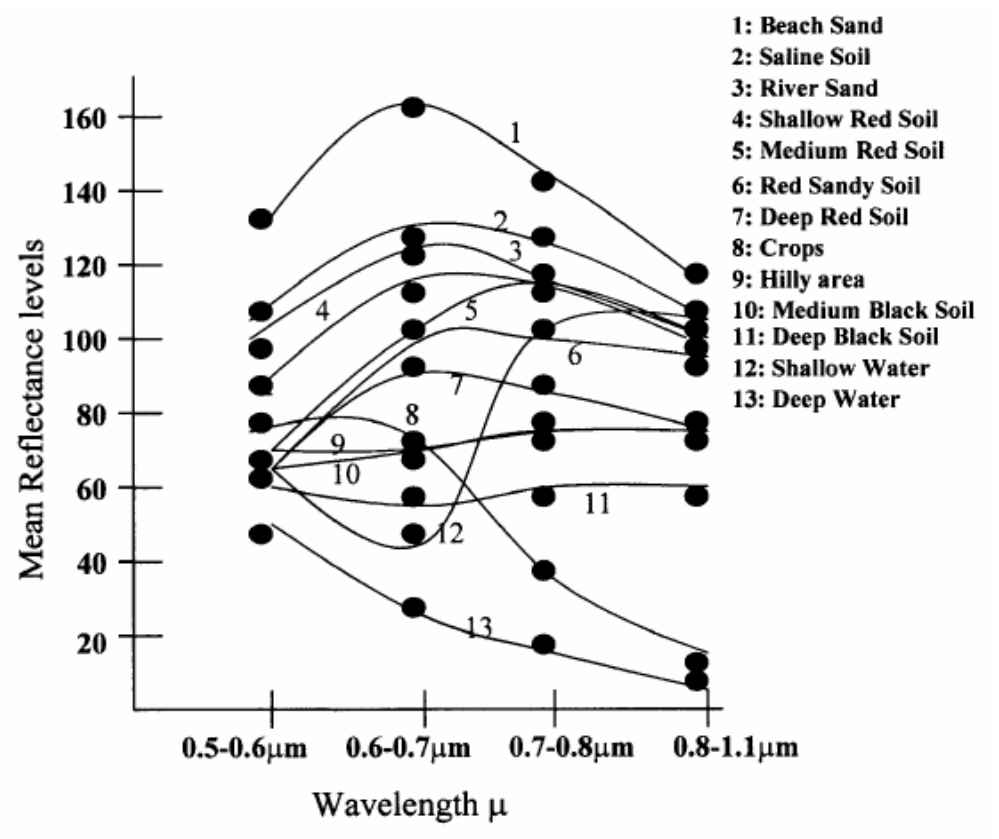

Fig. 3. Typical spectral curves for various soils and non soil classes (Source: Venkataratnam 1980).

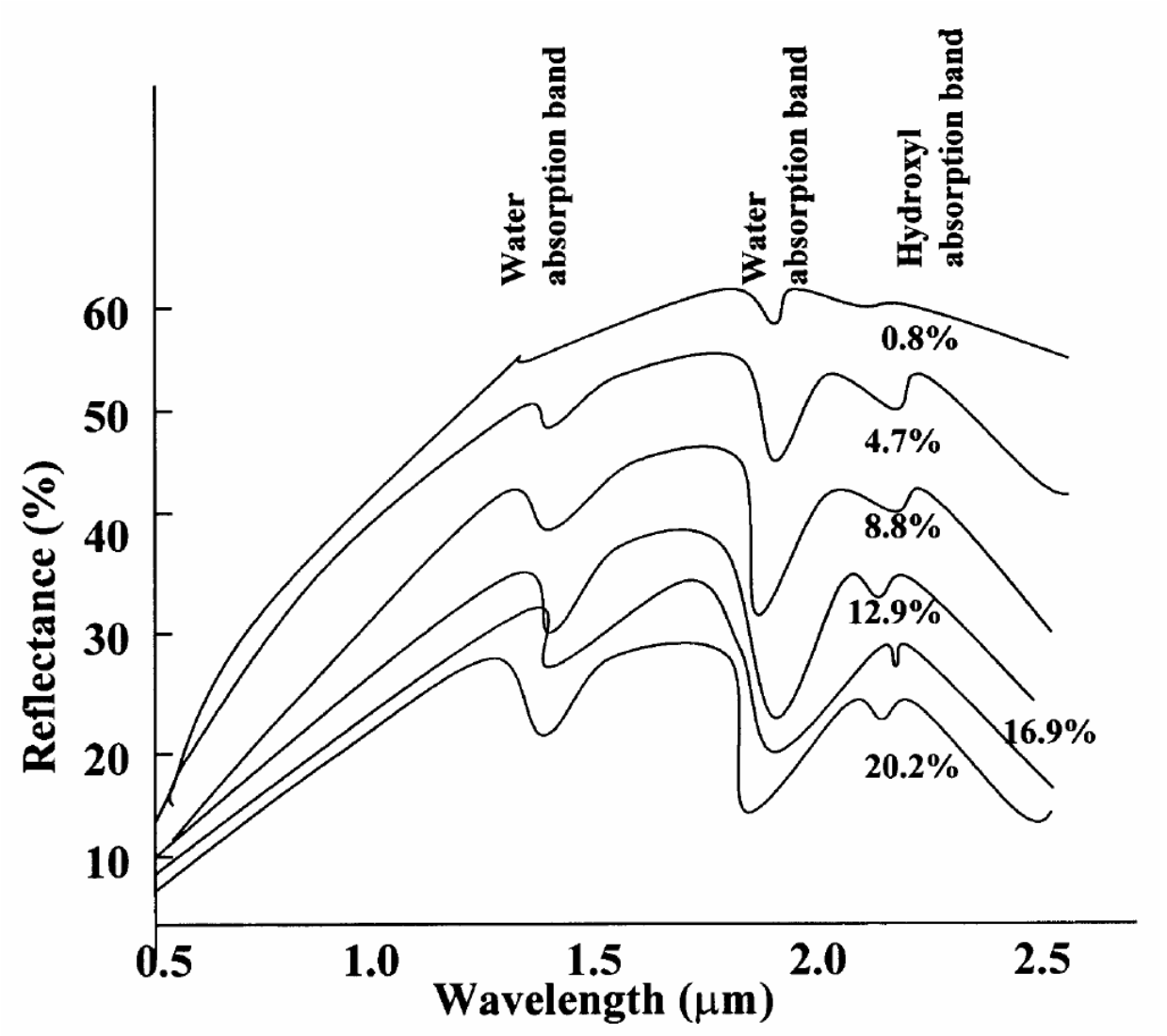

Fig. 2. Characteristic peaks of water and hydroxyl bonds (Source: Baumgardner *et al.* 1985).

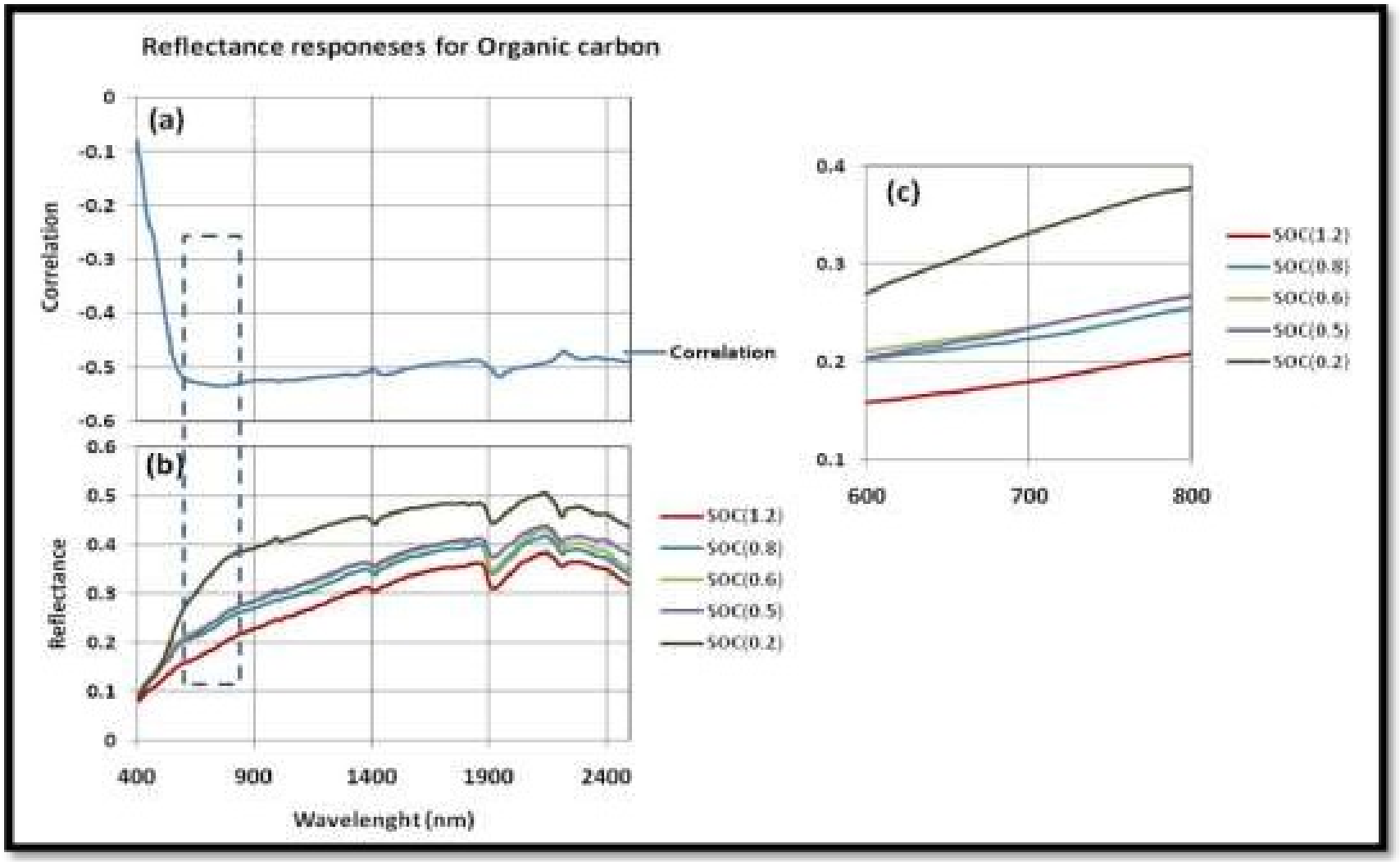

Spectral sensitivity analysis of Soil organic Carbon

Spectral features of soil

Objective/Phenomena	Relevant Spectra Region	Optimum Spectral Resolution
VIS (445 to 700 nm)		
Soil Colour	445nm	10-20 nm
Organic matter	490 nm	10-20 nm
Broadband absorption due to	520 nm	10-20 nm
(i) Fe-bearing minerals	565 nm	10-20 nm
(ii) Carbonates	620 nm	10-20 nm
(iii) Sulphate	670 nm	10-20 nm
Erosional features	683 nm	10-20 nm
NIR (745 TO 1035 nm)		
Vegetative cover	711 nm	10-20 nm
Human content	720 nm	10-20 nm
Weak absorption due to	780 nm	10-20 nm
Fe-bearing minerals	880 nm	10-20 nm
SiO^2	960 nm	10-20 nm
Erosional features	1035 nm	19-20 nm
SWIR 1: (1500 to 1800 nm)		
Soil moisture	1500 nm	350nm
(qualitative)	1680 nm	
Weak absorption bands of carbonates	1740 nm	10-20 nm
SWIR II (2000 TO 2400 NM)		
Characteristic absorption bands of $-CO^3$, -OH and	2320 nm	10 nm
SO^4 bearing minerals e.g. Carbonates and layer silicates	2310 nm	10 nm
-OH and AIOH bearing minerals e.g. kaolinite	2200 nm	10 nm
MuscoviteAlunite	2300 nm	10nm
MgOH bearing minerals e.g. Talc, Brucite	2340 nm	10 nm
	2400 nm	10 nm
Soil moisture	2160/2040 nm	20 nm

3000-5000 nm Atmospheric Window		
Characteristic emission	3400 nm	
Spectra	3400 nm	
Absorption bands due to		
(i) quartz	4000 nm	1000 nm
(ii) carbonates	4500 nm	1000-2000 nm
(iii) organic matter	4700	1000-2000 nm
8000-1400 nm Thermal Infrared Region		
Thermal inertia	10300-11300 nm	-
Emission spectra	11500-12500 nm	
Thermal regime (large scale)		
Microwave Region (1GHz to 20 GHz)		
Dielectric response	1.125 GHz (L band)	
Ionic conductivity (salinity)		
Soil moisture regime (smaller scale)	5.4 GHz (C-band)	
Profile moisture estimation	20 GHz (X-band)	
Erosion and micro-relief feature		

Structural soil crusts are relatively thin, dense, somewhat continuous layers of non-aggregated soil particles on the surface of tilled and exposed soils. Structural crusts develop when a sealed-over soil surface dries out after rainfall or irrigation.

This soil structural crust affect the some soil properties, such as infiltration, runoff and soil erosion

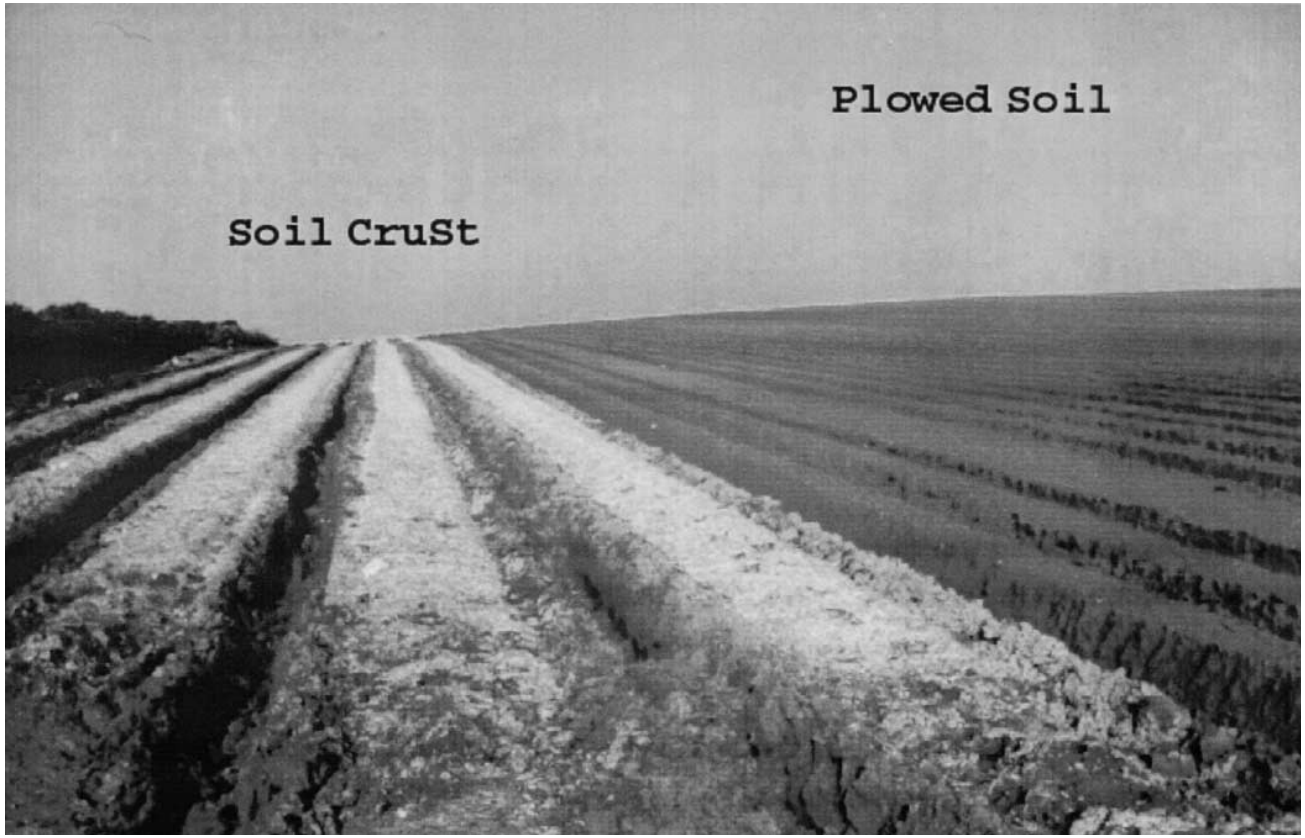

A field overview of Hamra soil after exposure to a natural rainstorm. Note the significant color differences between the crusted (light) and non crusted (dark) plowed soils.

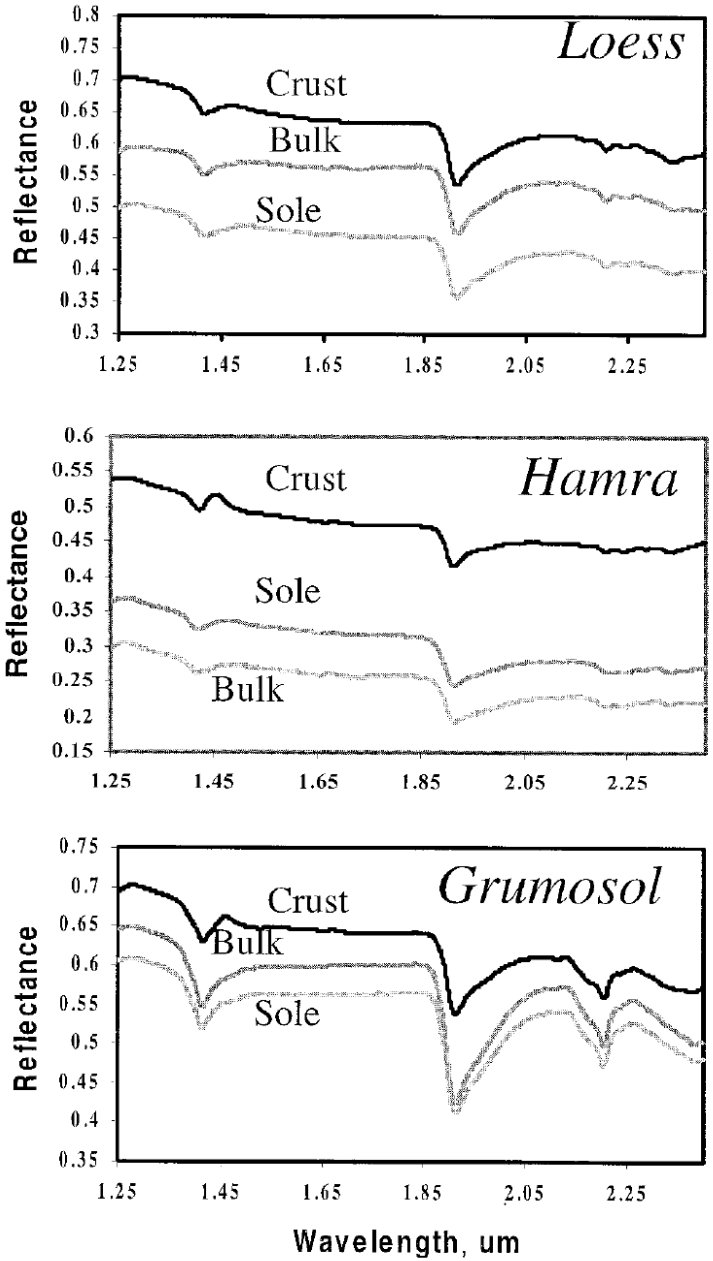

Fig. 2. Loess, Hamra, and Grumusol soil reflectance spectra at crust, sole, and bulk positions (see text for details).

Based on measurements of the three soils and their corresponding spectral fractions (crust, sole, and bulk, it is postulated that an albedo sequence occurs, moving from one fraction to another.

All crusts are characterized by relatively high reflectance values across the entire spectral region, whereas the sole fractions show relatively lower values.

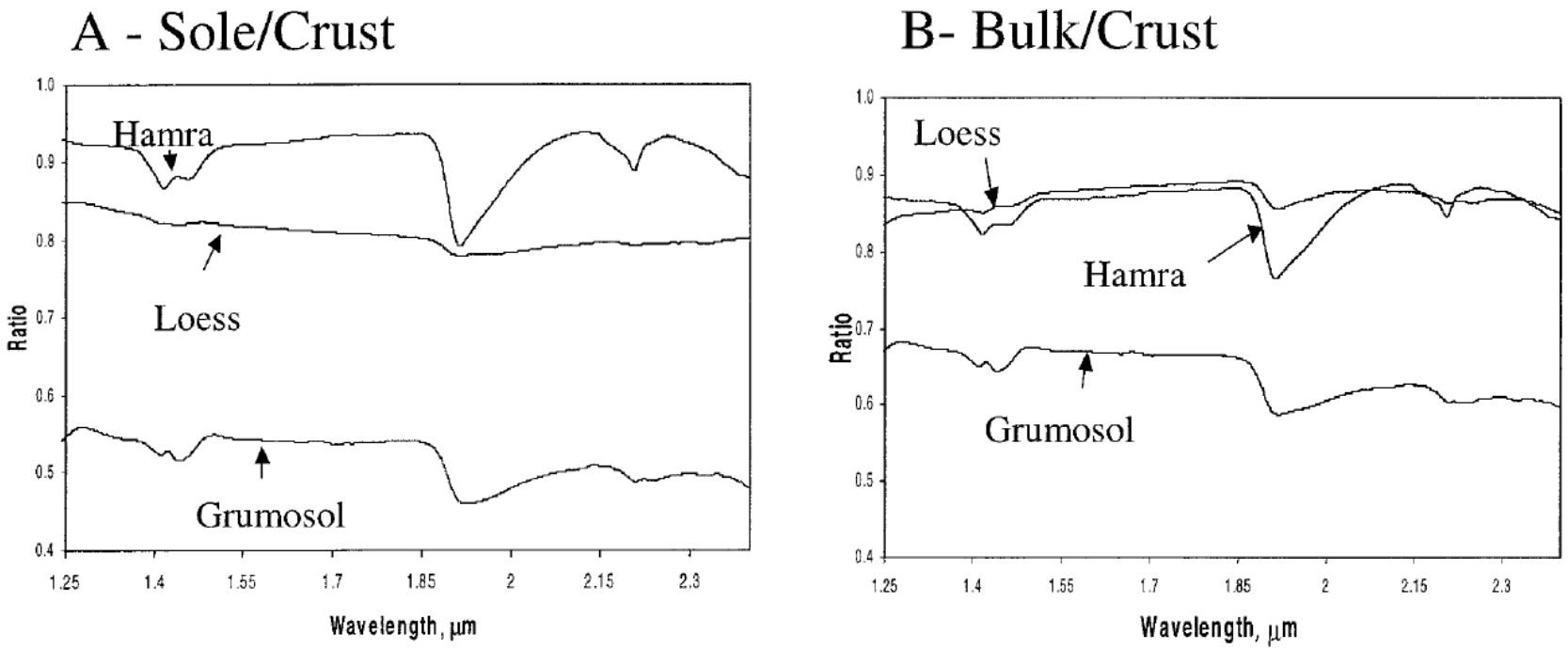

Fig. 3. The ratio between (A) sole and crust and (B) bulk and crust spectra of Hamra, Grumosol, and Loess soils.

Spectral signatures with the absorbance spectra of inorganic phosphates: the peaks at 1.4, 1.9 and 2.2 µm and the absorptions at 2.1 and 2.3 µm.

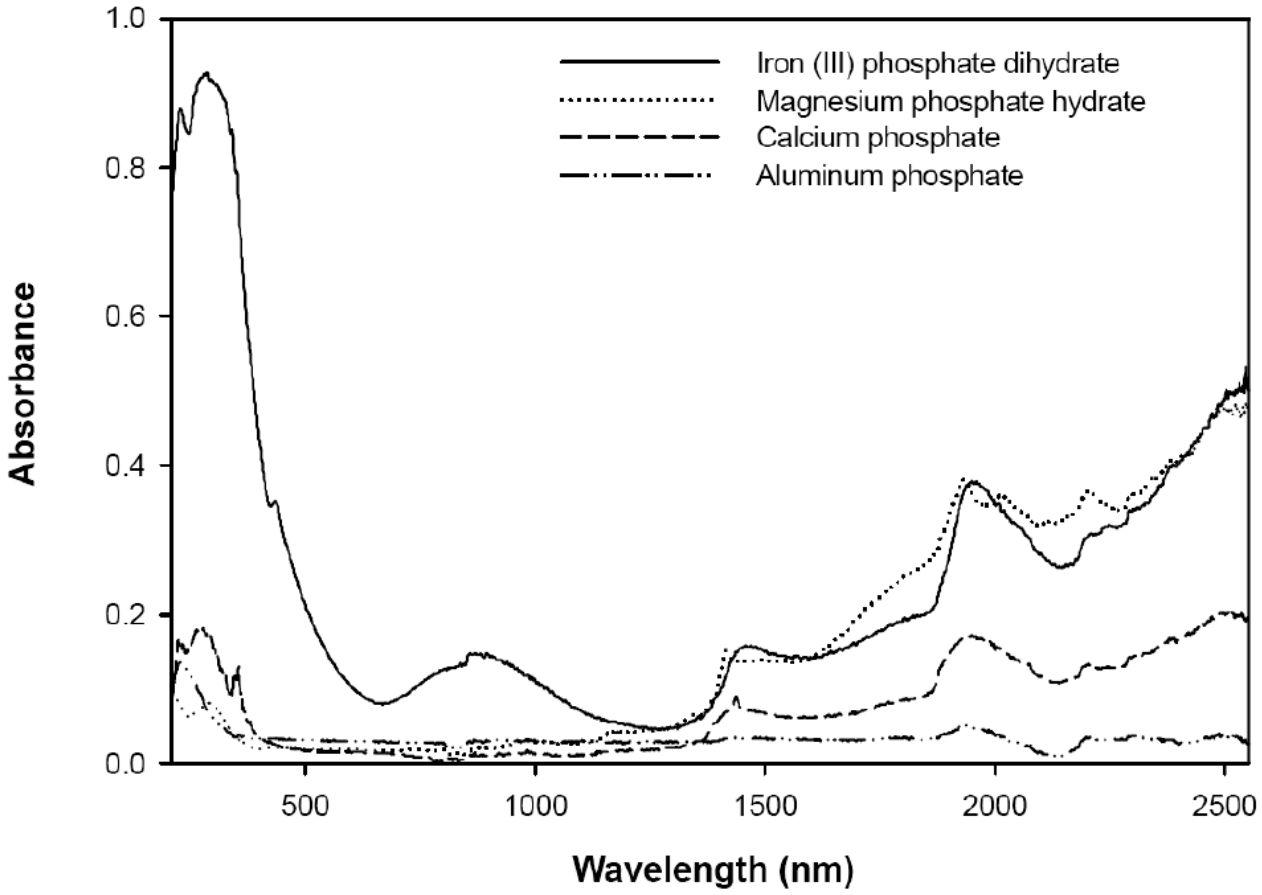

Figure 18. Absorbance of four P compounds in 208 - 2550 nm (from Brogrekci et al., 2005b)

HYPERSPECTRAL Remote sensing of water quality

Hyperspectral remote sensing can be used to estimate water quality parameters such as suspended sediments, turbidity, and chlorophyll

The use of remote sensing to quantify suspended sediment has been studied extensively

Suspended sediments increase the energy reflected from surface waters in the visible and nearinfrared spectrum. The specific amount of increase depends on sediment type, texture, color, water depth, and viewing conditions (Ritchie et al. 2003). Although reflectance increased at all wavelengths, Ritchie et al. (1976) concluded that wavelengths between 700 and 800 nm were most useful for quantifying suspended sediment concentration

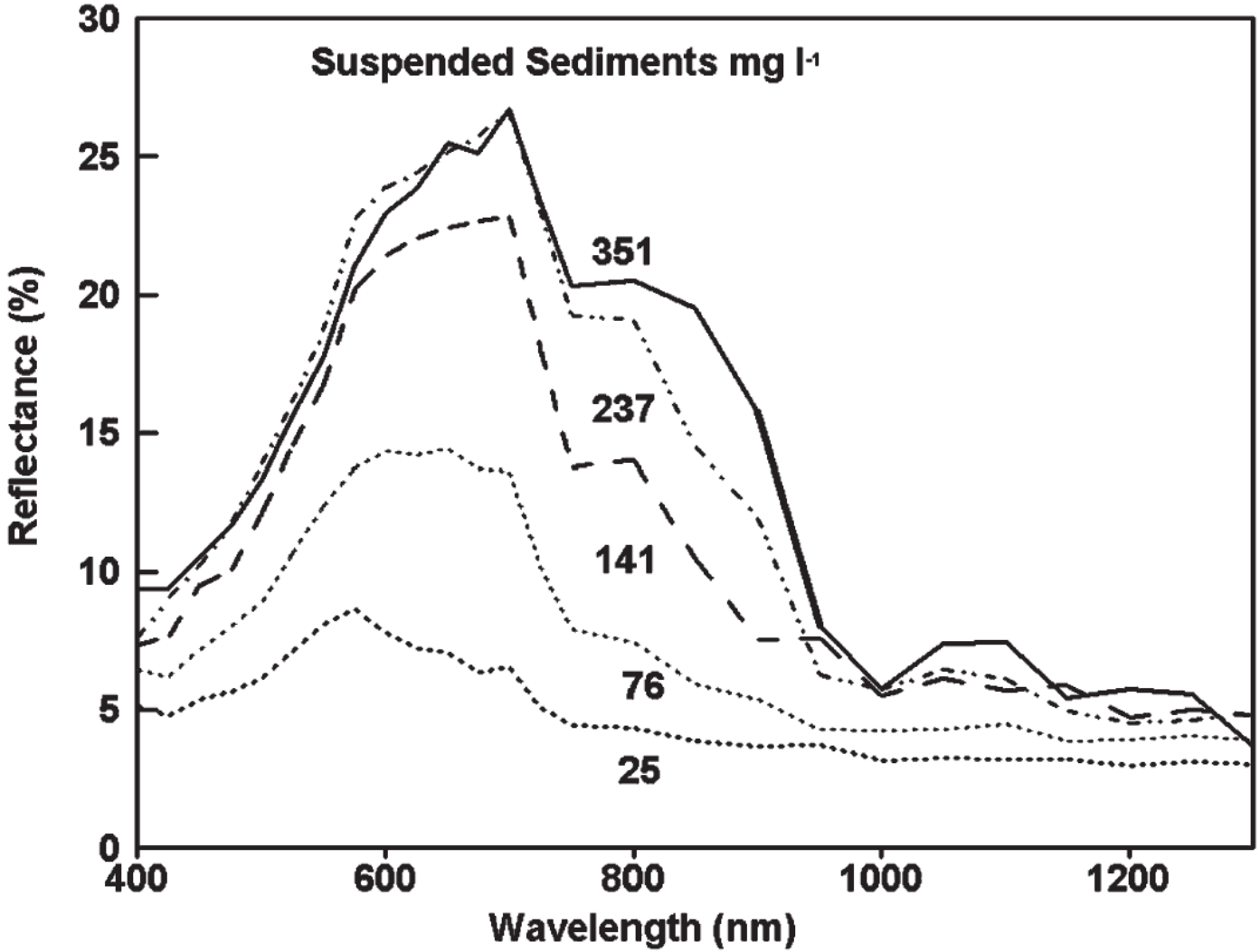

Figure 1. The relationship between reflectance and wavelength as affected by the concentration of suspended sediments (Ritchie *et al.*, 1976).

Ritchie et al. (1974) developed an empirical approach to estimate suspended sediments. The general forms of these empirical equations are

$$Y = A + BX \quad \text{or} \quad Y = AB^X$$

where *Y* is the remote sensing measurement (i.e., radiance, reflectance, energy) and *X* is the water quality parameter of interest (i.e., suspended sediment, chlorophyll). *A* and *B* are empirically derived factors. In empirical approaches statistical relationships are determined between measured spectral/thermal properties and measured water quality parameters.

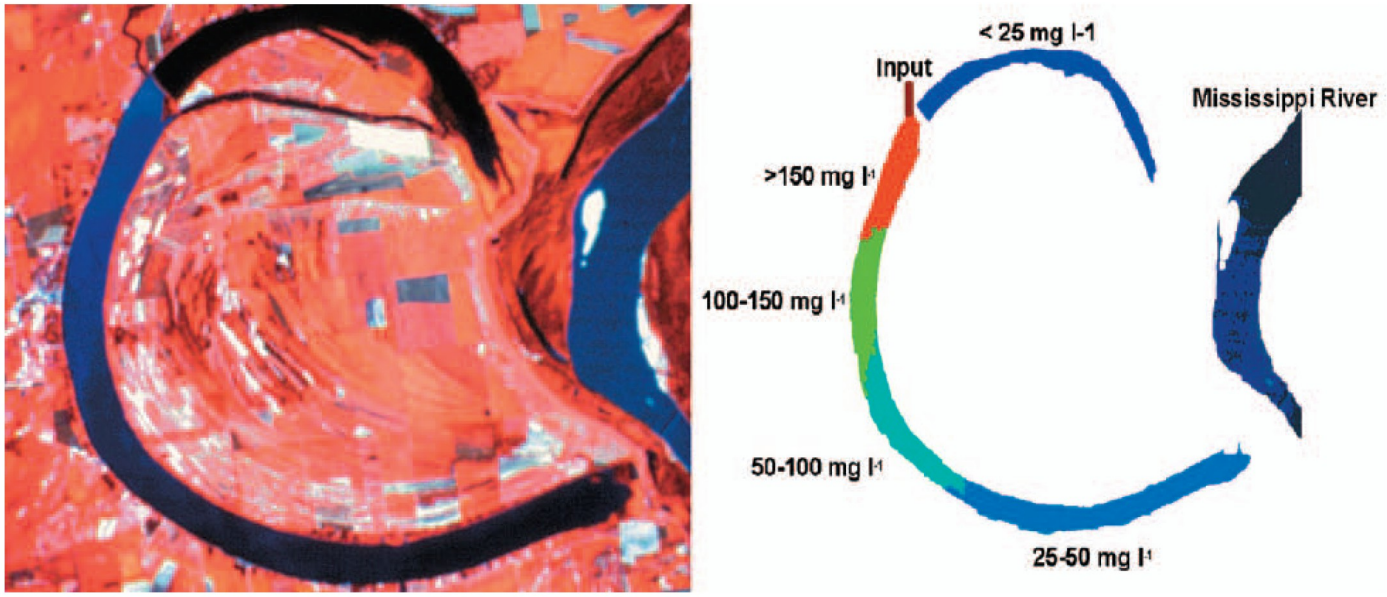

Plate 1. Landsat TM image of Lake Chicot, Arkansas (left) and a derived image (right) showing categories of suspended sediments mapped in Lake Chicot based on the radiance in the TM image.

Related to suspended sediment concentration is turbidity, a measure of the degree to which light transmitted through the water is scattered by suspended particles. Although turbidity is also influenced by the quantity and type of organic particulates (e.g., algae) in the water, suspended sediments are usually the dominant particulate matter in surface water, and therefore are the main cause of turbidity. The relationship between sediment concentration and turbidity is influenced by the particle size distribution of the sediment

Han (1996) achieved a correlation of 0.95 between turbidity and the difference in reflectance at 710 and 720 nm for samples obtained from a reservoir.

Several approaches used to estimate chlorophyll with remote sensing were reviewed by Ritchie et al. (2003). Multispectral approaches have not been successful in waters with high suspended sediment concentrations because these broad-wavelength data cannot successfully discriminate chlorophyll where the spectral signal is dominated by sediment.

However, research has shown that narrow-band reflectance data at the "red edge" of the visible spectrum can estimate chlorophyll in the presence of high suspended sediment concentrations.

This was particularly apparent when data from multiple measurement dates were combined (derivative r = 0.82; ratio r = 0.55). Shafique et al. (2003) used the 705/675 nm reflectance ratio to quantify chlorophyll *a* and reported similar results (r = 0.71 and 0.72) for two Ohio rivers.

Algae/Chlorophyll

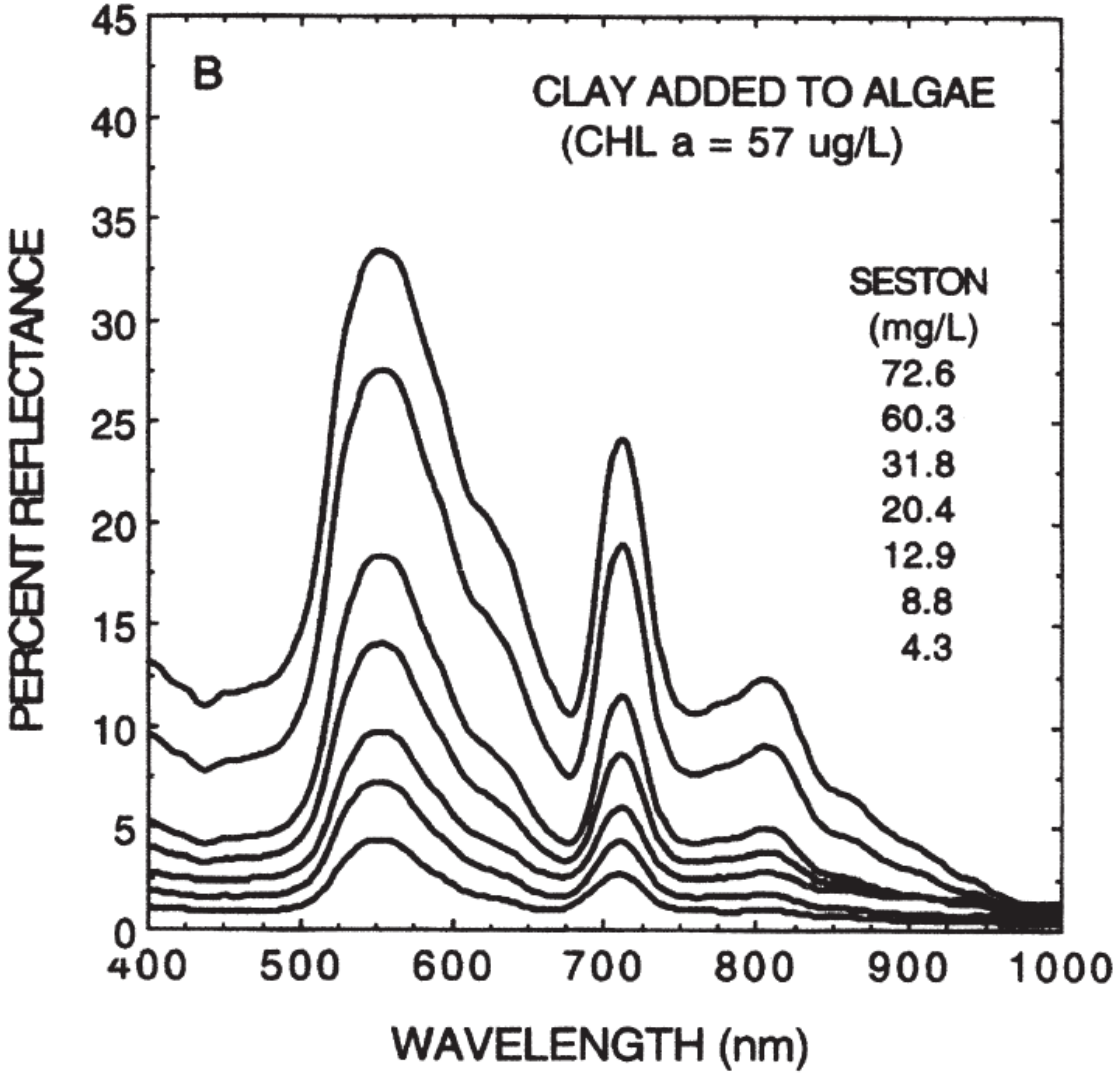

Figure 3. Relative contributions of chlorophyll and suspended sediment to a reflectance spectra of surface water. Based on *in situ* laboratory measurements made 1 m above the water surface by Schalles *et al.* (1997).

Monitoring the concentrations of chlorophyll (algal/phytoplankton) is necessary for managing eutrophication in lakes (Carlson 1977). Remote sensing has been used to measure chlorophyll concentrations spatially and temporally.

As with suspended sediment measurements, most remote sensing studies of chlorophyll in water are based on empirical relationships between radiance/reflectance in narrow bands or band ratios and chlorophyll

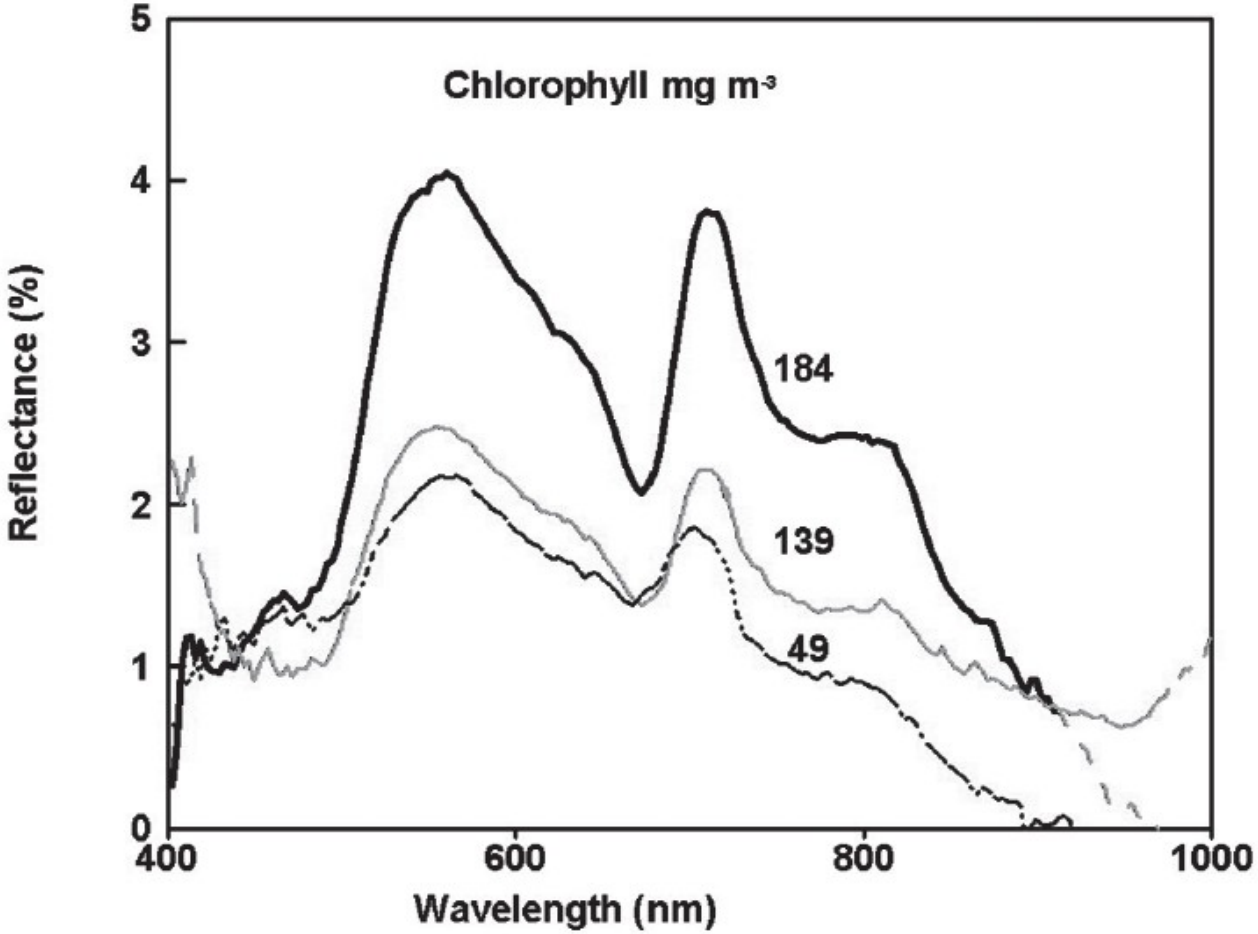

Figure 2. Relationship between reflectance and wavelength for different chlorophyll concentrations. Based on measurement made *in situ* with a high spectral resolution (1-nm) spectroradiometer at 1 meter over a large tank (Schalles *et al.*, 1997).